

SECOND ORDER CONE RELAXATIONS FOR QUANTUM MAX CUT

FELIX HUBER, KEVIN THOMPSON, OJAS PAREKH, AND SEVAG GHARIBIAN

ABSTRACT. Quantum Max Cut (QMC), also known as the quantum anti-ferromagnetic Heisenberg model, is a QMA-complete problem relevant to quantum many-body physics and computer science. Semidefinite programming relaxations have been fruitful in designing theoretical approximation algorithms for QMC, but are computationally expensive for systems beyond tens of qubits. We give a second order cone relaxation for QMC, which optimizes over the set of mutually consistent three-qubit reduced density matrices. In combination with Pauli level-1 of the quantum Lasserre hierarchy, the relaxation achieves an approximation ratio of 0.526 to the ground state energy. Our relaxation is solvable on systems with hundreds of qubits and paves the way to computationally efficient lower and upper bounds on the ground state energy of large-scale quantum spin systems.

Approximating the ground energy or state of a local Hamiltonian is a fundamental problem in quantum physics. While heuristic methods for providing upper bounds on the ground energy have been studied for many decades [CA86, Orú19, WRV⁺23, CT17], techniques for providing lower bounds have found mainly application in quantum chemistry [Maz09, NPA08, NNE⁺01, BH12, BP12, Fuk07, KSDN22]. Convex programs offer a systematic approach for relaxing both classical and quantum problems and obtaining such lower bounds. In particular, semidefinite programs (SDPs) are a natural fit for quantum mechanical problems as they allow modeling positivity of a state. Recently, Quantum Max Cut (QMC) has established itself as a test bed for *approximation algorithms* that provide rigorous bounds on the quality of the solution produced, with approximation algorithms [GP19, AGM20, PT22, Lee22, Kin23, LP24] based on noncommutative Lasserre SDP relaxations [PT21, TRZ⁺23, WCE⁺24, CJK⁺23] at the forefront. Quantum Max Cut problem is of particular interest because it models antiferromagnetic quantum spin systems through an equivalence with the quantum Heisenberg Hamiltonian, and it is a simple QMA-hard example of a 2-local Hamiltonian.

Given a graph (G, E) , quantum Max Cut problem asks for the ground state energy of the Hamiltonian

$$(1) \quad H = - \sum_{(ij) \in E} \frac{1}{2} (\mathbb{1} - \text{SWAP}_{ij}) w_{ij},$$

where the edge weights $\{w_{ij}\}_{(ij) \in E}$ are non-negative. The swap interaction expands in terms of Pauli matrices as $\text{SWAP} = \frac{1}{2} (\mathbb{1} \otimes \mathbb{1} + X \otimes X + Y \otimes Y + Z \otimes Z)$. We can thus write the QMC

Date: November 7, 2024.

We thank Ludovic Jaubert, Titus Neupert, Martin Plávala, and Claudio Procesi for fruitful discussions and helpful comments. This work is supported by a collaboration between the US DOE and other Agencies. FH was supported by the Foundation for Polish Science through TEAM-NET (POIR.04.04.00-00-17C1/18-00), Agence National de la Recherche (ANR-23-CPJ1-0012-01), and the Region Nouvelle-Aquitaine. This material is based upon work supported by the U.S. Department of Energy, Office of Science, Office of Advanced Scientific Computing Research, Accelerated Research in Quantum Computing, Fundamental Algorithmic Research for Quantum Computing (FAR-QC) and Fundamental Algorithmic Research toward Quantum Utility (FAR-Qu). This article has been authored by an employee of National Technology & Engineering Solutions of Sandia, LLC under Contract No. DE-NA0003525 with the U.S. Department of Energy (DOE). The employee owns all right, title and interest in and to the article and is solely responsible for its contents. The United States Government retains and the publisher, by accepting the article for publication, acknowledges that the United States Government retains a non-exclusive, paid-up, irrevocable, world-wide license to publish or reproduce the published form of this article or allow others to do so, for United States Government purposes. The DOE will provide public access to these results of federally sponsored research in accordance with the DOE Public Access Plan <https://www.energy.gov/downloads/doe-public-access-plan>.

Hamiltonian in Eq. (1) also as

$$(2) \quad H = -\frac{1}{4} \sum_{(i,j) \in E} (\mathbb{1} - X_i \otimes X_j - Y_i \otimes Y_j - Z_i \otimes Z_j) w_{ij}.$$

The QMC Hamiltonian tries to establish the maximally entangled singlet state $\frac{1}{\sqrt{2}}(|01\rangle - |10\rangle)$ on every pair of vertices connected by an edge. However, the monogamy of entanglement (or more formally, the quantum de Finetti theorem) forbids the sharing of maximal entanglement with multiple partners. This induces frustration into the ground states, and consequentially, not all terms in the Hamiltonian can simultaneously be minimized.

Remark 1. *Finding a ground state of the QMC Hamiltonian and the antiferromagnetic quantum Heisenberg model are equivalent since the Hamiltonians only differ in identity terms. However, from an approximation perspective, the two problems differ. Approximation guarantees for the Heisenberg model carry over to QMC but not vice versa.*

With exact diagonalization, the largest systems solved to date are 50 qubits using sublattice coding techniques [LSM19, WL18]. However, for disordered and large-scale systems such exact approaches fail due to the growing Hilbert space dimension and the lack of spatial symmetries. Variational algorithms can provide upper bounds, but work best on lattices in small dimensions.

Thus there is need for relaxations lower bounding the ground state energy. Such approaches roughly fall into two classes: a) quantum Lasserre or more general relaxations based on the NPA hierarchy [NPA08], which form moment matrices from the interaction algebra, and b) marginal approximations, which replace the optimization over ϱ by a set of mutually consistent marginals [Maz09, NNE⁺01, BH12, BP12, Fuk07, KSDN22].

Our contributions. The approach taken here is a mixture of the two types of approximation above: we optimize over a set of reduced density matrices (quantum marginals) that are mutually consistent as well as consistent with a Pauli level-1 quantum Lasserre moment matrix. Conceptually, this approach is similar to combining a classical Lasserre with Sherali-Adams hierarchy [SA90], with the difference that the local Sherali-Adams moment matrices are replaced by reduced density matrices.

First, we show that optimizing over mutually consistent 3-qubit reduced density matrices can be captured by a second order cone (SOC) program (Theorem B in Section 6). SOC are specializations of semidefinite programs that can be solved more efficiently in practice. In the process we show that a set of necessary constraints derived in [PT22] on the expectation values of 2-qubit quantum Max Cut terms are in fact sufficient (Theorem A in Section 5) and can be expressed as a second order cone constraint. This gives a concise description of the feasible space of expectation values for the three QMC terms on a triangle.

Second, we recall that the first level of the quantum Lasserre hierarchy yields a 0.498-approximation using product states [GP19], and a better approximation using only the first level is unlikely [HNP⁺23]. The second level of the quantum Lasserre hierarchy obeys certain monogamy of entanglement constraints [PT21, PT22], described in the next section, enabling better approximations, with 0.595 [LP24] the current best. However, the full generality of the second level of quantum Lasserre is not necessary to beat 0.498: we show that the first level along with our second order cone constraints yields a 0.526-approximation (Theorem 5 in Section 7).

On the practical side, we conduct a numerical study comparing our lower bounds with upper bounds obtained by state of the art methods on systems as large as 256 qubits (Section 9). In contrast, SDP relaxations, including the recently introduced optimized SWAP hierarchies for quantum Max Cut, are typically practically impractical beyond tens of qubits [TRZ⁺23, WCE⁺24]. Our numerics indicate that the relaxations we define are exact on Shastry-Sutherland models with small amounts of disorder (see Figure 4). Similar to previously defined relaxations [TRZ⁺23] we note that our hierarchy also “mimics” phase transitions in the Shastry-Sutherland model (see Figure 1).

Finally, we extend our relaxation to k -qubit marginals and local dimension $d > 2$ using the Weingarten formalism along with a new observation simplifying the approach.

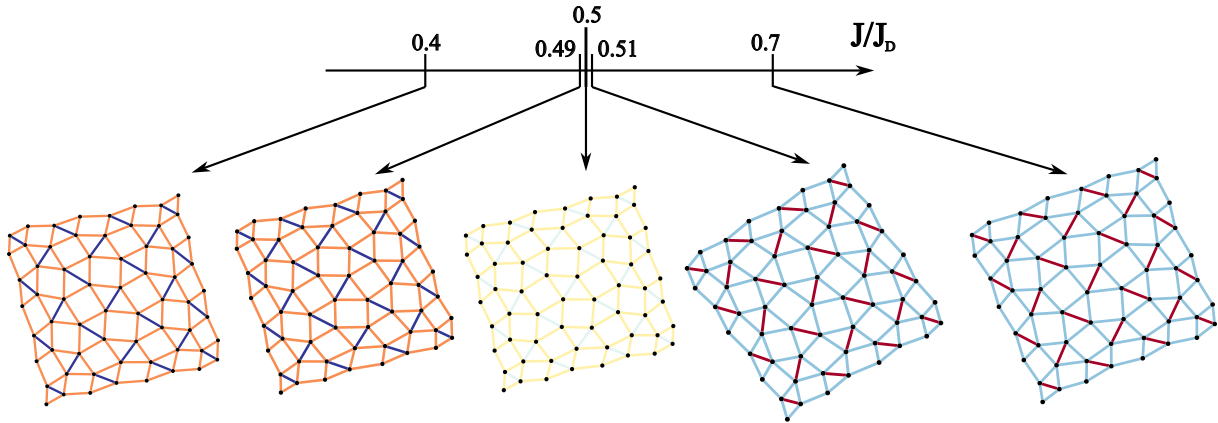


FIGURE 1. Phase transitions between Dimer–Plaquette–Néel phases in the Shastry–Sutherland model calculated from our SOCP relaxation [Equation (17)]. Dark blue edges indicate that the calculated objective along that edge is close to that of a singlet while dark red edges indicate that the objective is far from that of a singlet. Left: In the Dimer phase the ground state corresponds to a tensor product of singlet states along the blue edges. Center: The plaquette phase is an intermediate phase between these two extremes. Right: In the Néel phase the optimal state matches that of the square lattice, corresponding to aligned single qubit product states along the red edges. While our relaxations mimic the behavior of the physical model, they do not precisely match it. For the physical model the transient plaquette phase occurs in a larger parameter regime with the phase transitions at different points.

We hope for our relaxations to become a new tool for physicists studying disordered systems and structureless local Hamiltonians. Our methods can inherently handle arbitrary interaction graphs, including irregular lattice models, such as those modeling defects (Figure 2). These are typically hard to solve for variational methods due to lack of symmetry and locality.

1. MAIN RESULTS

Write $x = \langle \text{SWAP}_{12} \rangle$, $y = \langle \text{SWAP}_{13} \rangle$, and $z = \langle \text{SWAP}_{23} \rangle$. The Lieb–Mattis and Parekh–Thompson [PT22] conditions are:

$$(LM) \quad 0 \leq x + y + z \leq 3,$$

$$(PT) \quad (x^2 + y^2 + z^2) - 2(xy + xz + yz) + 2(x + y + z) \leq 3.$$

We show that (see Section 5):

Theorem A. *The Lieb–Mattis (LM) and Parekh–Thompson triangle (PT) inequalities form necessary and sufficient conditions for a real unitary-invariant trace one operator to represent a three-qubit quantum state.*

A second order cone program (SOCP) has form [LVBL98]

$$(3) \quad \begin{aligned} & \min_x f^T x \\ & \text{subject to} \quad \|A_i x + b_i\|_2 \leq c_i^T x + d_i, \quad i = 1, \dots, N, \end{aligned}$$

where $\|\cdot\|_2$ is the Euclidean norm. The variable $x \in \mathbb{R}^n$, and the problem parameters are $f \in \mathbb{R}^n$, $A_i \in \mathbb{R}^{n_i-1 \times n}$, $b_i \in \mathbb{R}^{n_i-1}$, $c_i \in \mathbb{R}^n$, and $d_i \in \mathbb{R}$. Equality constraints of the form $A_i x = -b_i$ can be included by setting $c_i = d_i = 0$ in (3). Second order cone programs can be solved with interior point algorithms and cover a larger class of problems than linear and quadratic programming. Yet, they are also strictly weaker than semidefinite programming (SDP) [Faw19] and typically require less computational effort than similarly structured semidefinite programs [AG03].

The Lieb-Mattis and Parekh-Thompson conditions can be formulated as SOC constraints. It follows that (see Section 6):

Theorem B. *Quantum Max Cut is lower bounded by a second order cone program in $\binom{n}{2}$ variables. It corresponds to optimizing over mutually consistent 3-qubit reduced density matrices.*

Here, mutually consistent means that the three-qubit density matrices (marginals) satisfy that $\text{tr}_k(\rho_{ijk}) = \text{tr}_\ell(\rho_{ik\ell})$ for all pairwise distinct $i, j, k, \ell \in \{1, \dots, n\}$. Naively, these are constraints on a collection of positive-semidefinite 8×8 matrices. We use the $U^{\otimes n}$ -invariance and realness of the QMC Hamiltonian to symmetry-reduce the positivity condition on a single three-qubit marginal to a linear and a second order cone constraint.

We combine this with the quantum Lasserre hierarchy: the idea is to consider a (pseudo-)moment matrix whose entries $\Gamma(E, F)$ correspond to expectations $\text{tr}(\rho E^\dagger F)$. As with a moment matrix coming from a state ρ , one requires that $\Gamma \succeq 0$ as well as all consistency constraints arising from the indexing set; e.g. from the relation $E^\dagger F = K^\dagger H$ follows the condition $\Gamma(E, F) = \Gamma(K, H)$. At level d , Γ is indexed by all Pauli strings of weight at most d . The Pauli level-1 quantum Lasserre relaxation then corresponds to optimizing a $3n \times 3n$ psd matrix. In combination with the second-order cone relaxation, one has an approximation guarantee (see Section 7):

Theorem C. *[see Theorem 5] The Pauli level-1 Lasserre hierarchy in combination with the second order cone program for mutually consistent 3-qubit reduced density matrices achieves an approximation ratio of 0.526.*

The best known approximation for QMC achieves a better approximation factor of 0.595 [LP24]. However, the rounding algorithm for this and prior work uses second level of the NPA hierarchy, with respect to either Pauli operators (so-called quantum Lasserre) or the first level of a hierarchy with respect SWAP operators. Either becomes intractable for instances as small as 20 qubits. We obtain a significant practical runtime improvement over all known approximation algorithms that approximate QMC to a factor at least 0.526.

Our symmetry-reduction can somewhat straightforwardly be extended to k -partite relaxations and dimension $d \geq 3$. We side-step the Weingarten formalism and simplify the expansion of the state by formulating positivity of an operator directly in terms of its expectation values $\langle \sigma \rangle = \text{tr}(\sigma A)$, $\sigma \in S_k$ (see Section 8).

Theorem D. *Let A be unitary invariant and R_μ be irreducible orthogonal representations. Then*

$$A \succeq 0 \quad \iff \quad \bigoplus_{\substack{\mu \vdash k \\ |\mu| \leq d}} \sum_{\sigma \in S_k} \langle \sigma \rangle R_\mu(\sigma) \succeq 0.$$

This avoids the computation of characters of the symmetric group and Schur polynomials in the usual expansion through the Weingarten formula.

2. PROOF IDEAS

Theorem A: Lieb-Mattis and Parekh-Thompson conditions. Consider a relaxation of the quantum Max Cut problem that optimizes over the set of mutually compatible reduced three-qubit density matrices. A result by Eggeling and Werner [EW01] shows that the any unitary-invariant three-qubit state can be block-diagonalized, so that the positivity of ρ_{ijk} corresponds to the positivity in two subspaces (formally, irrep). The first irrep is 1-dimensional, while the second is irrep is real and 2-dimensional, for which the positive semidefinite constraint can be formulated as a second order cone constraint. The third (completely anti-symmetric) irrep of the symmetric group S_3 vanishes and thus does not give a constraint on positivity.

Let us now see how the number of variables reduces from $3! = 6$ to 3: first, the vanishing irrep corresponds to the identity $\text{id} - (12) - (13) - (23) + (123) + (132) = 0$ for qubits. Furthermore, the QMC Hamiltonian is real and as a consequence $\langle (123) \rangle = \langle (132) \rangle \in \mathbb{R}$. This reduces the

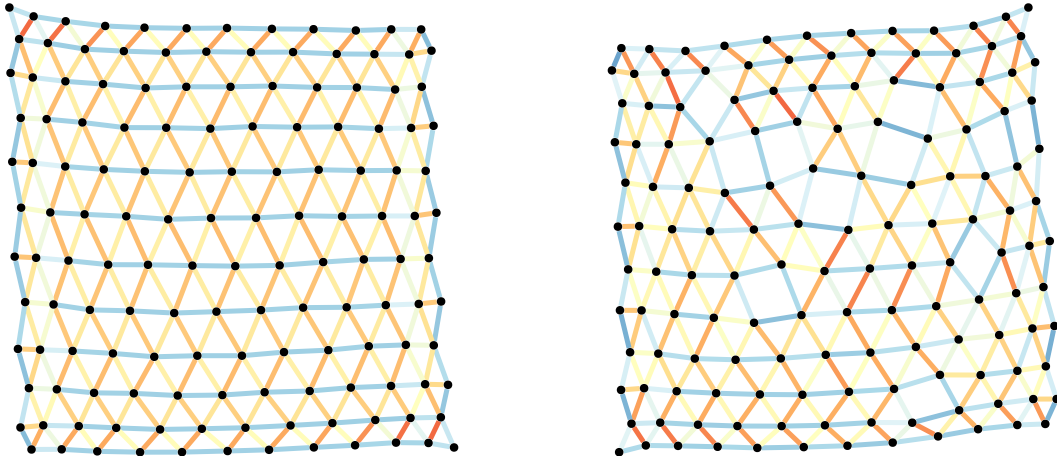


FIGURE 2. Approximations to quantum Max Cut on a 144-qubit lattice using the second order cone + Pauli level-1 relaxation. Shown are edge values that correspond to interaction terms in the Hamiltonian. Each subset of three vertices corresponds to a valid three-qubit reduced density matrix. A blue edge corresponds to the singlet state ($\langle \text{SWAP}_{ij} \rangle = -1$) and satisfies its edge constraint, showing no frustration. A red edge corresponds to a state orthogonal to the singlet ($\langle \text{SWAP}_{ij} \rangle = 1$) and indicates frustration. Compared to the lattice without defects where boundary effects dominate (right), lattice defects (left) curb the propagation of boundary effects into the interior, imposing local order.

number of variables to three and yields the LM and PT conditions for unitary-invariant operators of trace one.

Theorem B: Second-order cone relaxation. Considering all three-qubit subsystems, the consistent marginals relaxation consists of a second order cone program (SOCP) in $\binom{n}{2}$ real variables. Here each variable corresponds to a pair of vertices. A key ingredient to this second order cone program is to directly use the expectation values $\langle \text{SWAP}_{ij} \rangle = \text{tr}(\rho \text{SWAP}_{ij})$ instead of coefficients for an operator basis.

Theorem C: Approximation algorithm. Our approximation algorithm follows previous approaches, including the best-known 0.595 approximation, based on producing a state that is a tensor product of 1- and 2-qubit states. Being able to find a good product state solution is necessary in some regimes; for example, product states are approximately optimal as input graphs grow dense [BH16]. Level 1 of the quantum Lasserre hierarchy is necessary for a good product state approximation, and we add to this our second order cone constraints to form an SDP relaxation. All previous approaches use the LM condition on a star, while we can only enforce this on stars with two edges. This presents difficulties in obtaining a good approximation, requiring a new ingredient in our analysis. Ideally one would be able to show that a set of SDP relaxation values resulting in a bad approximation guarantee cannot occur as an optimal SDP solution for an actual input graph. Our analysis attempts to mimic this by keeping track of the fraction of edges with low, medium, or high SDP value and allows these fractions to be chosen adversarially.

Theorem D: symmetry-reduction of k-body marginals The usual expansion of an invariant operator reads in terms of expectation values as $\rho = \sum_{\pi \in S_k} \text{tr}(\rho \pi) \pi^{-1} \text{Wg}(d, n)$, where $\text{Wg}(d, n)$ is the Weingarten operator $\text{Wg}(d, k) = \frac{1}{k!} \sum_{\substack{\lambda \vdash k \\ |\lambda| \leq d}} \frac{\chi_\lambda(\text{id})}{s_{\lambda, d}(1)} p_\lambda$. Here χ_λ is the character of the symmetric group, $s_{\lambda, d} = s_\lambda(1, \dots, 1)$ (d times) the Schur polynomial, and P_μ is the central Young projector projecting onto the isotypic component labeled by μ . Theorem D then follows from the fact that $\text{Wg}(d, k)$ acts as a positive scalar on each non-vanishing isotypic component.

3. DISCUSSION

3.1. Higher dimensions and larger marginals. Naturally, a similar approach can be taken for quantum Max Cut on higher spin systems: Symmetry reduce the k -body marginals and demand their mutual consistency. However, not all nice features of the three-qubit relaxation carry through: For tri-partite system with $d \geq 2$ the partition $[1, 1, 1]$ does not vanish, and consequently the relaxation requires an extra variable $\langle(123)\rangle = \langle(132)\rangle \in \mathbb{R}$. The relaxation remains a second order cone program, now in four variables. However, already starting from $k = 4$ there are genuine semidefinite constraints appearing in the relaxation: the $[3, 1]$ partition of S_4 corresponds to a 3×3 semidefinite constraint. This makes the relaxations computationally less efficient.

Regarding a reduction in the number of variables, in the case of $d = 2$ (qubits), this can be achieved with the Involution Basis formed by $\{\sigma \in S_k | \sigma = \sigma^{-1}\}$ whose cardinality is the Catalan number $\binom{2n}{n}/(n+1)$ [Pro24]. In higher dimensions, the more general *Good Permutations* basis reduces the number of variables [Pro21].

3.2. Scaling. Most robust implementations solving SDP or SOCP rely on interior point methods. While the number of total interior point iterations can be comparable for the two, the key difference in complexity comes from testing whether a potential solution is feasible. In the SDP case, one must check that a matrix is positive semidefinite (PSD), while in the SOCP case, each SOC constraint can be checked in constant time in our case, and we have $O(n^3)$ such constraints, where n is the number of qubits. Checking feasibility of the second level of the (Pauli-based) quantum Lasserre hierarchy or the first level of the SWAP hierarchy entails checking that an $O(n^2) \times O(n^2)$ matrix is PSD. Even if we augment our SOCP only with the first level of the quantum Lasserre hierarchy, as is necessary for Theorem C, the cost becomes checking whether an $O(n) \times O(n)$ matrix is PSD and checking $O(n^3)$ constraints of constant size. Attempting to compute a Cholesky decomposition can be used to detect whether a matrix is PSD, and with this approach we get an $O(n^6)$ algorithm for checking feasibility for the quantum Lasserre or SWAP hierarchies, compared to $O(n^3)$ for our approach. Of course this worst-case complexity may not reflect empirical behavior; however, our numerical study support the hypothesis that our SOCP relaxation is significantly more efficient than solving more conventional SDP relaxations.

3.3. Outlook. Interestingly, the constraints corresponding to valid 3-body marginals coincide exactly with monogamy constraints found by Ref. [PT22] in the context of Lasserre relaxations. This raises the question at which point the quantum Lasserre relaxations become exact. Considering the Pauli Lasserre hierarchy alone, the rank loop condition [PNA10] in the Pauli hierarchy is met at level $\lceil n/2 \rceil$. To accurately represent a k -qubit system, one thus requires to solve for at most level $\lceil k/2 \rceil$. For hierarchies symmetrized to the Hamiltonian though, it is not clear at what level convergence should happen and it is surprising that this relatively simple relaxation is exact on three qubits. An interesting open direction is the understanding the minimal relations needed which coincide with the conditions for k -body marginals both for qubits and for $d \geq 3$.

The numerical results indicate that our relaxations can provide exact ground state energies for simple models with disorder and can also detect phase transitions. This adds to the growing body of evidence that convex relaxations can be powerful tools for physics and in particular for perturbation theory [Has24]. Our tools are particularly applicable to numerical study since second order cone programs are more efficient to solve than generic semi-definite programs.

4. CONCEPTS

4.1. Notation. We denote expectation values of observables A on a state ρ by $\langle A \rangle = \text{tr}(A\rho)$. Unless otherwise specified, we work with n -qubit systems on $(\mathbb{C}^2)^{\otimes n}$. The Pauli matrices are denoted by X, Y, Z ; when acting on a subsystem i as X_i, Y_i, Z_i . The variables $x_{ij} \in \mathbb{R}$ approximate expectation values $\langle \text{SWAP}_{ij} \rangle$ of swap operators SWAP_{ij} .

4.2. Permutations. The swap operator exchanges the two tensor factors of $\mathbb{C}^d \otimes \mathbb{C}^d$ as

$$(4) \quad \text{SWAP} |v\rangle \otimes |w\rangle = |w\rangle \otimes |v\rangle .$$

We use SWAP_{ij} to denote the action of SWAP on qubits i and j , i.e. the map

$$(5) \quad |v_1\rangle \otimes \dots \otimes |v_i\rangle \otimes \dots \otimes |v_j\rangle \otimes \dots \otimes |v_n\rangle \mapsto |v_1\rangle \otimes \dots \otimes |v_j\rangle \otimes \dots \otimes |v_i\rangle \otimes \dots \otimes |v_n\rangle.$$

Note that for $d = 2$,

$$(6) \quad \text{SWAP}_{ij} = \frac{1}{2} (I_i \otimes I_j + X_i \otimes X_j + Y_i \otimes Y_j + Z_i \otimes Z_j).$$

Since SWAP_{ij} acts as a transposition, it generates a representation T of the symmetric group S_n on $(\mathbb{C}^d)^{\otimes n}$. Its action is

$$(7) \quad T(\pi) |v_1\rangle \otimes \dots \otimes |v_n\rangle = |v_{\pi^{-1}(1)}\rangle \otimes \dots \otimes |v_{\pi^{-1}(n)}\rangle.$$

We denote the span of $\{T(\pi) | \pi \in S_n\}$ as Σ_n , and the subspace of symmetric matrices by $\Sigma_n^{\text{sym}} = \text{span}(\{A \in \Sigma_n | A^T = A\})$. We call operators satisfying $(U^{\otimes n})^\dagger B U^{\otimes n} = B$, $\forall U \in \mathcal{U}(d)$ as $U^{\otimes n}$ -invariant, or simply *unitary invariant*.

4.3. Schur-Weyl duality. The Schur-Weyl duality states that the commutant of the algebra Σ_n spanned by $\{T(\pi) : \pi \in S_n\}$ on the space $(\mathbb{C}^d)^{\otimes n}$ is the algebra spanned by $A^{\otimes n}$ with $A \in \text{GL}(d)$. The vector space then decomposes as

$$(8) \quad (\mathbb{C}^d)^{\otimes n} \simeq \bigoplus_{\substack{\lambda \vdash n \\ \text{height}(\lambda) \leq d}} \mathcal{U}_\lambda \otimes \mathcal{S}_\lambda.$$

where the diagonal action $A^{\otimes n}$ of the general linear group $\text{GL}(d)$ acts on \mathcal{U}_λ and the symmetric group as $T(\pi)$ on \mathcal{S}_λ . In particular, the QMC Hamiltonian is unitary-invariant, and so is its ground state. As a consequence, both can be expanded in terms of permutation operators.

5. THREE QUBITS

We now introduce the key component of our relaxation: a single three-qubit reduced density matrix, which can be understood as a ‘‘frustration triangle’’. Our aim is to solve this subsystem system exactly, so that it is consistent with all other three-qubit marginals. Henceforth, for simplicity we drop the $T(\pi)$ notation and denote permutations as products of cycles, e.g. (123), with id denoting the identity permutation.

5.1. Symmetry-reduction. In a seminal paper, Eggeling and Werner established a decomposition for tripartite unitary-invariant states [EW01] on $(\mathbb{C}^d)^{\otimes 3}$. A convenient basis for the invariant space is

$$(9) \quad \begin{aligned} R_+ &= \frac{1}{6} (\text{id} + (12) + (23) + (13) + (123) + (132)), \\ R_- &= \frac{1}{6} (\text{id} - (12) - (23) - (13) + (123) + (132)), \\ R_0 &= \frac{1}{3} (2 \text{id} - (123) - (132)), \\ R_1 &= \frac{1}{3} (2(23) - (13) - (12)), \\ R_2 &= \frac{1}{\sqrt{3}} ((12) - (13)), \\ R_3 &= \frac{i}{\sqrt{3}} ((123) - (132)). \end{aligned}$$

The projectors R_+ , R_- , and R_0 correspond to the three isotypic subspaces labeled by the partitions [3], [1, 1, 1], and [2, 1] respectively. The operators R_1, R_2, R_3 act as Pauli matrices on the subspace corresponding to projector R_0 . We use the following Lemma:

Lemma 2 (State characterization [EW01]). *For any operator ρ on $\mathcal{H}^{\otimes 3}$ define the six parameters $r_k = \text{tr}(\rho R_k)$, for $k = \{+, -, 0, 1, 2, 3\}$. Each unitary-invariant ρ is uniquely determined by the*

tuple $(r_+, r_-, r_0, r_1, r_2, r_3) \in \mathbb{R}^6$, and such tuple belongs to a density matrix in $\mathcal{H}^{\otimes 3}$ if and only if

$$(10) \quad r_+, r_-, r_0 \geq 0, \quad r_+ + r_- + r_0 = 1, \quad r_1^2 + r_2^2 + r_3^2 \leq r_0^2.$$

Identifying r_0, r_1, r_2, r_3 with the identity and the Pauli matrices, the last constraint corresponds to the (subnormalized) Bloch ball of a single qubit. The characterization in Lemma 2 requires six variables; we now reduce this to three variables: First, we show that we may assume that ϱ has real entries, and then we show that for real ϱ , three variables suffices.

5.2. Real weights. Consider a unitary-invariant three-qubit system on particles 1, 2, and 3. It can be expanded as

$$(11) \quad \varrho_{123} = \zeta \mathbb{1} + a(12) + b(23) + c(13) + d(123) + e(132),$$

where $a, b, c, d, e \in \mathbb{C}$. Now note that the swap operators $(12), (13), (23)$ are all Hermitian. Thus $\langle\langle ij \rangle\rangle \in \mathbb{R}$. But also $\langle\langle ijk \rangle\rangle \in \mathbb{R}$: The QMC Hamiltonian is real, $H^T = H$. This implies that also its ground state satisfies $\varrho = \varrho^T$. As a consequence,

$$(12) \quad \text{tr}(\varrho(123))^* = \text{tr}(\varrho^\dagger(123)^\dagger) = \text{tr}(\varrho(123)^T) = \text{tr}(\varrho^T(123)) = \text{tr}(\varrho(123)),$$

where we have used that the permutation operators are orthogonal and that $\pi^T = \pi^{-1}$. From the last equalities also $\langle\langle 123 \rangle\rangle = \langle\langle 132 \rangle\rangle \in \mathbb{R}$, which we use shortly.

5.3. Three-qubit identity. On the vector space $(\mathbb{C}^2)^{\otimes 3}$, the relation

$$(13) \quad \text{id} - (12) - (13) - (23) + (123) + (132) = 0$$

generates all nontrivial identities among the permutation operators [Pro07]. This simplifies the Werner-Eggeling basis further: From the matrix identity Equation (13) one has $r_- = \text{tr}(R_- \varrho) = 0$. From Equation (12) follows that $\langle\langle 123 \rangle\rangle = \langle\langle 132 \rangle\rangle$, and thus $r_3 = \text{tr}(R_3 \varrho) = 0$. Via Equation (13), the remaining operators R_+, R_0, R_1, R_2 simplify for QMC to:

$$(14) \quad \begin{aligned} R_+ &= \frac{1}{3}((12) + (13) + (23)), \\ R_0 &= \frac{1}{3}(3 \text{id} - (12) - (13) - (23)), \\ R_1 &= \frac{1}{3}(2(23) - (12) - (13)), \\ R_2 &= \frac{1}{\sqrt{3}}((12) - (13)). \end{aligned}$$

5.4. Lieb-Mattis and Parekh-Thompson conditions. For QMC, Lemma 2 simplifies to:

Corollary 3. *A real unitary-invariant operator in the span of R_0, R_1, R_2, R_+ corresponds to a three-qubit state, if and only if the following conditions are met:*

$$(15) \quad 0 \leq r_+ \leq 1, \quad r_+ + r_0 = 1, \quad r_1^2 + r_2^2 \leq r_0^2.$$

Now write $x = \langle\langle 12 \rangle\rangle$, $y = \langle\langle 23 \rangle\rangle$, and $z = \langle\langle 13 \rangle\rangle$. Assume $\langle\langle \mathbb{1} \rangle\rangle = 1$. Then Corollary 3 reads:

$$(LM) \quad 0 \leq x + y + z \leq 3,$$

$$(PT) \quad (x^2 + y^2 + z^2) - 2(xy + xz + yz) + 2(x + y + z) \leq 3,$$

The bound (LM) is known as Lieb-Mattis inequality and corresponds to $0 \leq r_+ \leq 1$, and (PT) as the Parekh-Thompson triangle inequality corresponding to $r_1^2 + r_2^2 \leq r_0^2 = (1 - r_0)^2$. The latter was discovered through an analysis of the second level of the quantum Lasserre hierarchy in Pauli polynomials [PT22, Lemma 7], but as we have shown here, it can also be obtained as a consequence of [EW01]. We have thus shown the following:

Theorem A. *The Lieb-Mattis (LM) and Parekh-Thompson triangle (PT) inequalities form necessary and sufficient conditions for a real unitary-invariant trace one operator to represent a three-qubit quantum state.*

To see that any single of these constraints are sufficient (for trace one operators), consider the projectors R_+ and R_0 onto the subspaces corresponding to the partitions $[3]$ and $[2, 1]$ respectively. One can check that $\frac{1}{2}R_+ - \frac{1}{4}R_0$ is a trace one operator satisfying (PT) but not (LM), while $\frac{1}{12}(R_0 + 2(12))$ is a trace one operator satisfying (LM) but not (PT).

Note that Thm. A assumes the operator to be of trace one: there exist non-normalized operators (e.g. $-R_0$) that satisfy both inequalities but that are not positive semidefinite. However, if for a given set of $x, y, z \in \mathbb{R}$ (LM) and (PT) are satisfied, then there exists an operator in the hyperplane of trace one that is a state.

A natural question is how these conditions generalize to the case of k -body marginals for dimensions $d > 2$. As we show in Section 8, every unitary-invariant k -body reduced density matrix can be decomposed into irreps of the symmetric group S_k . Demanding positivity in each irreducible component with overall trace one yields necessary and sufficient conditions for an operator to be a state. These are generally positive semidefinite cone constraints, which in the case of real 2×2 matrices reduce to a second order cone. Further simplifications, that is reducing the number of variables, can be made when $d < k$ by including identities that correspond to partitions that lie in the kernel of the representation of the symmetric group. In Section 5.3 this is done in the case of three qubits, for which the representation of the partition $[1, 1, 1]$ vanishes.

6. SECOND ORDER CONE RELAXATION

We now use the representation of a real unitary-invariant three-qubit state to provide a relaxation to QMC corresponding to optimizing over mutually constituent three-qubit marginals.

6.1. Compatible marginals. Consider now an instance of quantum Max Cut on a graph (G, E) with n vertices. We demand that the approximation to the ground state satisfies:

- (1) all three-party subsystems ϱ_{ijk} are density matrices on $(\mathbb{C}^2)^{\otimes 3}$;
- (2) every pair of three-qubit subsystems are compatible on their joint two-qubit reductions.

We arrive at the following semidefinite programming relaxation to the optimization in Eq. (1):

$$\begin{aligned}
 \min_{\{\varrho_{ijk}\}} \quad & -\frac{1}{2} \sum_{(i,j) \in E} \text{tr}((1 - \text{SWAP}_{ij})\varrho_{ij}) \\
 \text{subject to} \quad & \varrho_{ij} = \text{tr}_k(\varrho_{ijk}), \\
 & \varrho_{ijk} \geq 0 \\
 & \text{tr}(\varrho_{ijk}) = 1, \\
 (16) \quad & \text{tr}_k(\varrho_{ijk}) = \text{tr}_\ell(\varrho_{ij\ell}), \quad k \neq \ell.
 \end{aligned}$$

where the sum and constraints are over all pairwise different $i, j, k \in \{1, \dots, n\}$. This relaxation contains $\binom{n}{3}$ complex SDP variables of size 8×8 . We now show how it can be symmetry reduced to $\binom{n}{2}$ real variables, with $\binom{n}{3}$ linear programming constraints and $\binom{n}{3}$ second-order cone constraints.

6.2. Symmetry reduction. We now reduce the size of the coupled SDP constraints. To every pair (i, j) of vertices associate a variable $x_{ij} \in \mathbb{R}$ representing the expectation value $\langle \text{SWAP}_{ij} \rangle$. If $x_{ij} = -1$ then ϱ_{ij} is in the singlet state. The SWAP operator has eigenvalues $\{+1, -1\}$ and thus we have the constraint $-1 \leq x_{ij} \leq 1$. It follows from Theorem A that the semidefinite program of Equation (16) can be relaxed to:

$$\begin{aligned}
 \min_{\{x_{ij}\}} \quad & -\frac{1}{2} \sum_{(i,j) \in E} (1 - x_{ij}) \\
 \text{subject to} \quad & 0 \leq x_{ij} + x_{jk} + x_{ik} \leq 3, \\
 (17) \quad & (x_{ij}^2 + x_{ik}^2 + x_{jk}^2) - 2(x_{ij}x_{ik} + x_{ij}x_{jk} + x_{ik}x_{jk}) + 2(x_{ij} + x_{ik} + x_{jk}) \leq 3
 \end{aligned}$$

As desired, this SDP yields a set of three-qubit density matrices that are mutually consistent on all two-qubit marginals, and whose objective value lower bounds the ground state energy of quantum Max Cut.

6.3. Second order cone relaxation. A second order cone program (SOCP) has form [LVBL98]

$$(18) \quad \begin{aligned} & \min_x f^T x \\ & \text{subject to} \quad \|A_i x + b_i\|_2 \leq c_i^T x + d_i, \quad i = 1, \dots, N, \end{aligned}$$

where $\|\cdot\|_2$ is the Euclidean norm. The variable $x \in \mathbb{R}^n$, and the problem parameters are $f \in \mathbb{R}^n$, $A_i \in \mathbb{R}^{n_i-1 \times n}$, $b_i \in \mathbb{R}^{n_i-1}$, $c_i \in \mathbb{R}^n$, and $d_i \in \mathbb{R}$. Equality constraints of the form $A_i x = -b_i$ can be included by setting $c_i = d_i = 0$ in (18).

Note that Eq. (17) [respectively the last constraint in Eq. (15)] is a second order cone constraint,

$$(19) \quad \|A_{ijk} \vec{x}_{ijk} + b_{ijk}\| \leq c_{ijk} \vec{x}_{ijk} + d_{ijk}, \quad 1 \leq i < j < k \leq n.$$

with

$$(20) \quad \vec{x}_{ijk} = \begin{pmatrix} x_{ij} \\ x_{ik} \\ x_{jk} \end{pmatrix}, \quad A_{ijk} = \frac{1}{3} \begin{pmatrix} -1 & -1 & 2 \\ \sqrt{3} & -\sqrt{3} & 0 \end{pmatrix}, \quad c_{ijk} = \frac{1}{3} \begin{pmatrix} -1 \\ -1 \\ -1 \end{pmatrix}, \quad b_{ijk} = d_{ijk} = 0.$$

This gives the following result:

Theorem B. *Quantum Max Cut is lower bounded by a second order cone program in $\binom{n}{2}$ variables. It corresponds to optimizing over mutually consistent 3-qubit reduced density matrices.*

6.4. Why SOCP. On a conceptual level, why does a second order cone constraint appear in our relaxation? The reason is that the positivity condition of a single three-qubit marginal decomposes into a linear constraint on the [3] partition, and a positive semidefinite constraint on the 2-dimensional [2, 1] partition,

$$(21) \quad \begin{pmatrix} r_0 + r_1 & r_2 \\ r_2 & r_0 - r_1 \end{pmatrix} \succeq 0.$$

By the determinant test it is clear that this constraint is equivalent to $r_1^2 + r_2^2 \leq r_0^2$ with $r_0 - r_1 \geq 0$ and $r_0 + r_1 \geq 0$.

7. APPROXIMATION ALGORITHM

We will find it convenient to cast QMC as maximization problem, by negating the terms in (1), so that energies are nonnegative.

7.1. Relaxation. The quantum Lasserre hierarchy indexing by polynomials in Pauli matrices can be used to strengthen the SOCP relaxation. Consider three moment matrices with entries

$$(22) \quad M_{ij}^X = \text{tr}(X_i X_j \rho), \quad M_{ij}^Y = \text{tr}(Y_i Y_j \rho), \quad M_{ij}^Z = \text{tr}(Z_i Z_j \rho),$$

where X_i, Y_i, Z_i are single Pauli operators on position i . It is clear that $M^X, M^Y, M^Z \succeq 0$. Then consider their sum $M = M^X + M^Y + M^Z$, which by Equation (6) has the properties

$$(23) \quad M \succeq 0, \quad M_{ii} = 3, \quad M_{ij} = 2x_{ij} - 1.$$

With this additional semidefinite constraint, the relaxation (17) is strengthened to:

$$(24) \quad \begin{aligned} & \max_{x_{ij}} \quad \frac{1}{2} \sum_{(i,j) \in E} (1 - x_{ij}) \\ & \text{subject to} \quad 0 \leq x_{ij} + x_{jk} + x_{ik} \leq 3, \\ & \quad (x_{ij}^2 + x_{ik}^2 + x_{jk}^2) - 2(x_{ij}x_{ik} + x_{ij}x_{jk} + x_{ik}x_{jk}) + 2(x_{ij} + x_{ik} + x_{jk}) \leq 3 \\ & \quad M \succeq 0, \quad M_{ii} = 3, \quad M_{ij} = 2x_{ij} - 1. \end{aligned}$$

7.2. Algorithm and approximation guarantee. The recent design of approximation algorithms for Quantum Max Cut has exposed new connections between convex programming relaxations of local Hamiltonians and monogamy of entanglement. In particular, the second level of the quantum Lasserre hierarchy in Pauli polynomials enforces the Lieb-Mattis inequality on stars in the interaction graph (this inequality for stars with two edges follows from (LM)) [PT21]. This star bound has been instrumental in designing approximation algorithms for Quantum Max Cut, and seems to be a necessary ingredient in obtaining good approximation algorithms using entangled states. We will work with variables $y_{ij} = \frac{1}{2}(1 - x_{ij}) = \text{tr}(\frac{1}{2}(\mathbb{1} - \text{SWAP}_{ij})\rho)$, for a state ρ , corresponding to the negative of Quantum Max Cut Hamiltonian terms (1). The y_{ij} variables will also correspond to relaxed values in the context of our SOCP and SDP relaxations. The analog of equations (LM) and (PT) in y_{ij} variables are

$$\begin{aligned} \text{(LM')} \quad & 0 \leq y_{ij} + y_{jk} + y_{ik} \leq \frac{3}{2} \\ \text{(PT')} \quad & y_{ij}^2 + y_{jk}^2 + y_{ik}^2 \leq 2(y_{ij}y_{jk} + y_{ij}y_{ik} + y_{jk}y_{ik}) \end{aligned}$$

Lemma 4 (Star bound, Theorem 11 in [PT21]). *Let $y_{ij} \in [0, 1]$ for all $(i, j) \in E$ correspond to values on Quantum Max Cut Hamiltonian terms from the second level of the quantum Lasserre hierarchy in Pauli polynomials. Then for each $i \in V$,*

$$(25) \quad \sum_{j \in N(i)} y_{ij} \leq \frac{|N(i)| + 1}{2},$$

where $N(i) = \{j : (i, j) \in E\}$ denotes the neighborhood of i . Equivalently,

$$(26) \quad - \sum_{j \in N(i)} x_{ij} \leq 1.$$

Approximation algorithms for Quantum Max Cut hinge on a selection of an appropriate ansatz for output states. For product states, an α -approximation algorithm for Quantum Max Cut, with $\alpha \approx 0.498$, is best possible [HNP⁺23], and an α -approximation is possible using the first level of the Pauli-based quantum Lasserre hierarchy [GP19]. An optimal $\frac{1}{2}$ -approximation using product states is possible by employing the star bound and the Parekh-Thompson triangle inequality [PT22]. Anshu, Gosset, and Morenz [AGM20] observed that the $\frac{1}{2}$ -approximation barrier could be surmounted by using tensor products of 1- and 2-qubit states, which can be produced by finding matchings¹ in the interaction graph G . Given a matching M , placing singlets on edges $e \in M$ yields a state. The currently best known 0.595-approximation by Lee and Parekh is obtained by simply taking the better of the state obtained from a maximum matching in G or the product state obtained by the Gharibian-Parekh α -approximation on a solution from the second level of the Pauli hierarchy [LP24].

The star bound, particularly in the form of (26), illustrates connections to matching, where for a matching M , we must have, for $i \in V$, $\sum_{j \in N(i)} m_{ij} \leq 1$ if $m_{ij} \in \{0, 1\}$ are variables indicating $ij \in M$. Our SDP or SOCP relaxations do not imply the star bound, and in absence of it, proving approximation guarantees beyond 0.498 is challenging using existing techniques [GP19, PT21, PT22, Lee22, Kin23, LP24]. As with previous approaches, our algorithm outputs a product state as well as a state derived from a matching. However, in addition we introduce a new technique that allows us to get a 0.526-approximation with respect to our SDP relaxation (24). Previous approaches have used SDP values on edges to decide how to round to a quantum state. While these values depend on the input graph G , the relationship is not direct. Ideally one would be able to show that a set of SDP values resulting in a bad approximation guarantee cannot occur as an optimal SDP solution for an actual input graph. Our analysis attempts to mimic this by keeping track of the fraction of edges with low, medium, or high SDP value and allows these fractions to be chosen adversarially.

We obtain the following approximation result.

¹A matching of G is a subset of edges such that no two edges in the subset share a common vertex.

Algorithm 1 SOCP Approximation Algorithm

Input: Graph $G = (V, E)$, edge weights $\{w_{ij}\}_{ij \in E}$, threshold $t > 3/4$

- 1: Solve (24) using graph G and edge weights $\{w_{ij}\}_{ij \in E}$ to obtain optimal variable values $(M, \{y_{ij}\}_{ij \in E})$.
- 2: Construct $S = \{ij \in E : y_{ij} > t\}$ (guaranteed to be a matching by Equation (26) since $y_{ij} > 3/4$ implies $-x_{ij} > 1/2$)
- 3: Compute Cholesky decomposition of M to obtain vectors $\{|v_i\rangle \in \mathbb{R}^{|V|}\}$ such that $M_{ij} = \langle v_i | v_j \rangle$.
- 4: Sample $R \in \mathbb{R}^{3 \times |V|}$ by sampling matrix elements R_{ij} as i.i.d. standard normal random variables.
- 5: For each $k \in V$ define $(\theta_X^k, \theta_Y^k, \theta_Z^k) = R |v_k\rangle / \|R |v_k\rangle\|_2$.
- 6: Define $\varrho_S = \prod_{ij \in S} \left(\frac{\mathbb{I} - X_i X_j - Y_i Y_j - Z_i Z_j}{4} \right) \prod_{k: ik \notin S \forall i} \left(\frac{\mathbb{I} + \theta_X^k X_k + \theta_Y^k Y_k + \theta_Z^k Z_k}{2} \right)$
- 7: Define $\varrho_{prod} = \prod_{k \in V} \left(\frac{\mathbb{I} + \theta_X^k X_k + \theta_Y^k Y_k + \theta_Z^k Z_k}{2} \right)$.
- 8: **return** $\max\{\text{tr}(H\varrho_S), \text{tr}(H\varrho_{prod})\}$

Theorem 5. For $t = 0.771$, Algorithm 1 is a 0.526 approximation algorithm for Quantum Max Cut.

Lemma 6. Let $\{y_e\}_{e \in E}$ and M be derived from a feasible solution to (24). Given a feasible solution let $\{(\theta_X^k, \theta_Y^k, \theta_Z^k)\}_{k \in V}$ be sampled as in Algorithm 1 and define

$$F(x) := \frac{1}{4x} \left(1 - \frac{8}{9\pi} {}_2F_1 \left(\frac{1}{2}, \frac{1}{2}; \frac{5}{2}; \frac{1}{9}(1-4x)^2 \right) \right),$$

where ${}_2F_1$ is the Hypergeometric function.

(1) [GP19, BOFV14]

$$\mathbb{E}_R \left(\frac{1 - \theta_X^i \theta_X^j - \theta_Y^i \theta_Y^j - \theta_Z^i \theta_Z^j}{4Y_{ij}} \right) = F \left(\frac{1 - M_{ij}}{4} \right).$$

(2) [GP19] $F(x) \geq 0.498$ for $x \in (0, 1]$.

(3) $F(x)$ is monotonically decreasing in the interval $(0, 4/5]$.

(4) [LP24] If $y_{ij} \geq 3/4$ then $y_{jk} \leq 1/4(3 - 2y_{ij} + 2\sqrt{3}\sqrt{y_{ij} - y_{ij}^2})$.

Proof. Only Item 3 requires a proof². Let q be shorthand for $\frac{1}{3}(1-4x)$. Using the known derivative $\frac{d}{dz} {}_2F_1(a, b; c; z) = \frac{ab}{c} {}_2F_1(a+1, b+1; c+1; z)$ [AS48] we may compute

$$(27) \quad \frac{dF}{dx} = \frac{32xq^2 {}_2F_1\left(\frac{3}{2}, \frac{3}{2}; \frac{7}{2}; q^2\right) + 40 {}_2F_1\left(\frac{1}{2}, \frac{1}{2}; \frac{5}{2}; q^2\right) - 45\pi}{180\pi x^2} =: \frac{g(x)}{180\pi x^2}.$$

We can see that $\frac{dF}{dx} \leq 0$ for all $x \in (0, 4/5]$ if and only if $g(x) \leq 0$ for all $x \in (0, 4/5]$. We may compute

$$(28) \quad \frac{dg}{dx} = -\frac{384}{7}x(1-4x) \left(3q^2 {}_2F_1\left(\frac{5}{2}, \frac{5}{2}; \frac{9}{2}; q^2\right) + 7 {}_2F_1\left(\frac{3}{2}, \frac{3}{2}; \frac{7}{2}; q^2\right) \right).$$

By the series expansion ${}_2F_1(z) = \sum_{n=0}^{\infty} \frac{(a)_n (b)_n z^n}{(c)_n n!}$, one can see that $(3q^2 {}_2F_1(\frac{5}{2}, \frac{5}{2}; \frac{9}{2}; q^2) + 7 {}_2F_1(\frac{3}{2}, \frac{3}{2}; \frac{7}{2}; q^2))$ is non-negative where defined since ${}_2F_1(z^2)$ is a series of non negative terms. Note $x \leq 4/5$ by assumption so ${}_2F_1(5/2, 5/2; 9/2, 1/9(1-4x)^2)$ is always defined. Hence $dg/dx \leq 0$ for $x \leq 1/4$ and $dg/dx \geq 0$ for $1/4 \leq x \leq 4/5$. It follows that $g(x) \leq \max\{g(0), g(0.8)\}$ for $x \in [0, 4/5]$. $g(0)$ and $g(4/5)$ can be computed to show $g(x) \leq 0$ for all $x \in [0, 4/5]$ which implies $dF/dx \leq 0$ for all $x \in (0, 4/5]$. This implies F is monotonically decreasing in this interval. \square

²Technical lemmas very similar to Item 3 were used in other works [HNP⁺23, PT22, PT21], but we could not find anything which explicitly implies Item 3.

Proof of Theorem 5. For each edge e let G_e^S be the expected value of edge e obtained by the rounding algorithm for the state ϱ_S and let G_e^{prod} be defined analogously. Let S be the set of edges with $y_e > t$, T be the set of edges adjacent to S , and U be the set of edges not included in and not adjacent to S . Since $t = 0.771$, by Lemma 6 Item 4, edges $e \in T$ have values $y_e \leq t' = 1/4(3 - 2t + 2\sqrt{3}\sqrt{t - t^2}) \approx 0.728$.

First consider the approximation ratio for ϱ_{prod} .

$$(29) \quad \begin{aligned} \frac{\sum_e w_e G_e^{prod}}{\sum_e w_e y_e} &= \sum_e \left(\frac{w_e y_e}{\sum_{e'} w_{e'} y_{e'}} \right) \frac{G_e^{prod}}{y_e} = \sum_e \alpha_e \frac{G_e^{prod}}{y_e} \\ &= \sum_{e \in S} \alpha_e \frac{G_e^{prod}}{y_e} + \sum_{e \in T} \alpha_e \frac{G_e^{prod}}{y_e} + \sum_{e \in U} \alpha_e \frac{G_e^{prod}}{y_e}. \end{aligned}$$

By Lemma 6 Item 1 $G_e^{prod}/y_e = F(y_e)$. Since $F(x)$ is monotonically decreasing by Lemma 6 Item 3 we may lower bound $G_e^{prod}/y_e \geq F(t)$ for $e \in U$ and $G_e^{prod}/y_e \geq F(t')$ for $e \in T$. By Lemma 6 Item 2 we may lower bound $G_e^{prod}/y_e \geq 0.498$ for $e \in S$. Hence,

$$(30) \quad \frac{\sum_e w_e G_e^{prod}}{\sum_e w_e y_e} \geq \alpha 0.498 + \beta F(t') + \gamma F(t),$$

for $\alpha = \sum_{e \in S} \alpha_e$, $\beta = \sum_{e \in T} \alpha_e$ and $\gamma = \sum_{e \in U} \alpha_e$.

Now consider ϱ_S . $G_e^S/y_e \geq 1$ for $e \in S$ since ϱ_S is a singlet along that edge, $G_e^S/y_e \geq 1/4$ for $e \in T$ since one endpoint of edge e is involved in a singlet state and $G_e^S/y_e \geq F(t)$ for $e \in U$ by Lemma 6 Item 1. Similar reasoning yields

$$(31) \quad \frac{\sum_e w_e G_e^S}{\sum_e w_e y_e} \geq \alpha + \frac{\beta}{4} + \gamma F(t).$$

If we denote G_e as the expected edge value from the overall algorithm then

$$(32) \quad \frac{\sum_e w_e G_e}{\sum_e w_e y_e} \geq \frac{\max\{\sum_e w_e G_e^{prod}, \sum_e w_e G_e^S\}}{\sum_e w_e y_e} \geq \max\left\{ \frac{\sum_e w_e G_e^{prod}}{\sum_e w_e y_e}, \frac{\sum_e w_e G_e^S}{\sum_e w_e y_e} \right\}.$$

By (30) and (31),

$$(33) \quad \frac{\sum_e w_e G_e}{\sum_e w_e y_e} \geq \max\{0.498\alpha + \beta F(t') + \gamma F(t), \alpha + \frac{\beta}{4} + \gamma F(t)\}.$$

Since $\sum_e \alpha_e = 1$ and each $\alpha_e \geq 0$ we can lower bound the approximation factor for the overall algorithm as

$$(34) \quad r := \min_{\substack{\alpha + \beta + \gamma = 1 \\ \alpha, \beta, \gamma \geq 0}} \max\{0.498\alpha + \beta F(t') + \gamma F(t), \alpha + \frac{\beta}{4} + \gamma F(t)\}.$$

r may be solved with a linear program

$$(35) \quad \begin{aligned} r &= \min_{\alpha, \beta, \gamma, s} s \\ \text{subject to} \quad & 0.498\alpha + \beta F(t') + \gamma F(t) \leq s \\ & \alpha + \frac{\beta}{4} + \gamma F(t) \leq s \\ & \alpha + \beta + \gamma = 1 \\ & \alpha, \beta, \gamma \geq 0. \end{aligned}$$

We obtain $r = 0.526$.

□

8. K-BODY RELAXATIONS

We generalize the three-qubit state constraints to k -body reduced density matrices with $d \geq 2$. Theorem D characterizes positivity of an invariant operator directly from its expectation values and might be of independent interest.

8.1. Weingarten expansion. One can expand a unitary-invariant operator as [CS06, Pro21]

$$(36) \quad A = \sum_{\sigma \in S_k} \text{tr}(\sigma^{-1} A) \sigma \text{Wg}(d, n),$$

where the Weingarten operator is given by

$$(37) \quad \text{Wg}(d, k) = \frac{1}{k!} \sum_{\substack{\lambda \vdash k \\ |\lambda| \leq d}} \frac{\chi_\lambda(\text{id})}{s_{\lambda, d}(1)} p_\lambda.$$

Here χ_λ is the character of the symmetric group, $s_{\lambda, d} = s_\lambda(1, \dots, 1)$ (d times) the Schur polynomial, and the central Young projectors defined by

$$(38) \quad p_\lambda = \frac{\chi_\lambda(\text{id})}{k!} \sum_{\pi \in S_k} \chi_\lambda(\pi^{-1}) \pi.$$

we can write the Weingarten operator as

$$(39) \quad \text{Wg}(k, d) = \frac{1}{(k!)^2} \sum_{\substack{\lambda \vdash k \\ |\lambda| \leq d}} \frac{\chi_\lambda(\text{id})^2}{s_{\lambda, d}(1)} \sum_{\pi \in S_k} \chi_\lambda(\pi^{-1}) \pi.$$

With this we can expand Eq. (36) as

$$(40) \quad A = \sum_{\sigma, \tau \in S_k} \text{tr}(\sigma^{-1} A) \tau \text{Wg}(\tau^{-1} \sigma, d)$$

where, using the fact that $\chi_\lambda(\pi) = \chi_\lambda(\pi^{-1})$, the Weingarten function is

$$(41) \quad \text{Wg}(\pi, d) = \frac{1}{(k!)^2} \sum_{\substack{\lambda \vdash k \\ |\lambda| \leq d}} \frac{\chi_\lambda(\text{id})^2}{s_{\lambda, d}(1)} \chi_\lambda(\pi).$$

Expansion (40) has the drawback that it requires to compute the Weingarten operator respectively function. We address this in Section 8.3, Theorem D.

8.2. Symmetry reduction. Let $A \in \Sigma_{k, d}$ and R_λ be an orthogonal representation corresponding to λ . By the Schur-Weyl decomposition in Eq. (8),

$$(42) \quad T \mapsto \bigoplus_{\lambda \vdash k, |\lambda| \leq d} R_\lambda$$

is a $*$ -isomorphism. This preserves positivity [BGSV12], and thus

$$(43) \quad A = \sum_{\pi \in S_k} a_\pi T(\pi) \succeq 0 \quad \iff \quad \bigoplus_{\substack{\lambda \vdash k \\ |\lambda| \leq d}} \sum_{\pi \in S_k} a_\pi R_\lambda(\pi) \succeq 0.$$

In terms of the expectation values $\text{tr}(\pi A)$, the coefficients a_π are given in terms of expectation values $\langle \sigma^{-1} \rangle = \text{tr}(\sigma^{-1} A)$ as

$$(44) \quad a_\pi = \sum_{\sigma \in S_k} \text{tr}(\sigma^{-1} A) \text{Wg}(\pi^{-1} \sigma, d).$$

8.3. Direct decomposition. Eq. (44) suggests that Weingarten function has to be evaluated to test for positivity given expectation values. We now show how a more direct decomposition can be made which avoids this. The key idea is that the Weingarten operators scales each isotypic component λ by a positive scalar, and that $R_\mu(p_\lambda) = \delta_{\mu\lambda}\mathbb{1}$. Now use the fact that p_λ is in the center of the group ring $\mathbb{C}[S_n]$,

$$(45) \quad \begin{aligned} A &= \sum_{\sigma \in S_k} \text{tr}(\sigma^{-1}A)\sigma \text{Wg}(d, n) \\ &= \frac{1}{k!} \sum_{\substack{\lambda \vdash k \\ |\lambda| \leq d}} \frac{\chi_\lambda(\text{id})}{s_{\lambda,d}(1)} p_\lambda \sum_{\sigma \in S_k} \text{tr}(\sigma^{-1}A)\sigma \end{aligned}$$

Then

$$(46) \quad A \succeq 0 \iff \bigoplus_{\substack{\mu \vdash k \\ |\mu| \leq d}} \frac{1}{k!} \sum_{\substack{\lambda \vdash k \\ |\lambda| \leq d}} \frac{\chi_\lambda(\text{id})}{s_{\lambda,d}(1)} R_\mu \left(p_\lambda \sum_{\sigma \in S_k} \text{tr}(\sigma^{-1}A)\sigma \right) \succeq 0.$$

We simplify this expression in two steps: First note that the centrally primitive idempotents project onto the isotypic components labeled by λ and thus $R_\lambda(p_\mu) = \mathbb{1}\delta_{\lambda\mu}$. This can be seen by the fact that p_λ projects onto a minimal left ideal of $\mathbb{C}S_n$, while R_μ is an irreducible representation of S_n . Under a representation, left ideals are mapped to invariant subspaces; and when the ideal is minimal then its representation is either irreducible or zero. Thus when $\lambda = \mu$, then $R_\lambda(p_\lambda)$ acts as the identity onto the subspace λ , and when $\lambda \neq \mu$ then $R_\mu(p_\lambda) = 0$. Consequentially, $R_\lambda(p_\mu) = \mathbb{1}\delta_{\lambda\mu}$. Second, when $|\lambda| \leq d$ then $\frac{\chi_\lambda(\text{id})}{s_{\lambda,d}(1)} > 0$ is a positive number.

As a consequence, we have the following simplification of Eq. (43) respectively Eq. (46):

Theorem D. *Let A be unitary invariant and R_μ be irreducible orthogonal representations. Then*

$$A \succeq 0 \iff \bigoplus_{\substack{\mu \vdash k \\ |\mu| \leq d}} \sum_{\sigma \in S_k} \langle \sigma \rangle R_\mu(\sigma) \succeq 0.$$

8.4. Variable reduction. The ground state of the Quantum Max Cut Hamiltonian has real coefficients $a_\pi = a_\pi^{-1} \in \mathbb{R}$. To see this, note that $H^T = H$. The ground state can thus be chosen to satisfy the same symmetry. Consequently, $\varrho^T = \varrho$. Then

$$(47) \quad \text{tr}(\varrho\pi)^* = \text{tr}(\varrho^\dagger \pi^\dagger) = \text{tr}(\varrho\pi^T) = \text{tr}(\varrho^T \pi) = \text{tr}(\varrho\pi).$$

Thus the expectation values are real, $\langle \pi \rangle \in \mathbb{R}$. In Eq. (43) the expectation values are multiplied by the Weingarten function in Eq. (41) which is also real. Thus the coefficients satisfy $a_\pi = a_{\pi^{-1}} \in \mathbb{R}$ for all $\pi \in S_k$.

A more systematic variable reduction can be done through the identities generated by the projector R_- onto the anti-symmetric subspace of three systems. An alternative is to use the *Good Permutations* basis [Pro21] works for general d but is overcomplete in the case of symmetric matrices.

9. NUMERICAL RESULTS

In this section we detail some numerical results on the performance of our relaxations. We primarily investigated (1) the performance of our graph relative to known variation benchmarks [WRV+23] (VarBench) (2) the performance/behavior on the Shastry-Sutherland model [SS81] and (3) the performance on random (Erdos-Renyi) graphs.

In the first set of benchmarks we compared our relaxations to known ground states and heuristically derived solutions for a subset of lattices covered in [WRV+23]. For these results the QMC Hamiltonian is scaled to be traceless, i.e. $H = \sum_{ij \in E} X_i X_j + Y_i Y_j + Z_i Z_j$. Our calculations were all completed on a mid-range workstation without supercomputing resources in contrast to [WRV+23]. In particular with a Intel(R) Xeon(R) Gold 6258R processor and 64 GB of RAM. We stress additionally that our methods are complementary to [WRV+23] since we provide lower rather than upper bounds on the ground state energy (which is normally achieved

with heuristics). One peculiar feature of the optimal solutions we calculated was that in many cases the optimal solution (in the VarBench scaling) is exactly minus the number of edges. In the context of Equation (17) this corresponds to setting all x_{ij} variables to 1. This will always be a feasible solution to these programs so the optimal solution of the relaxation will always be smaller than the number of edges. We compared the relaxation strengths and computation times of SOC and SOC+P1 to the level-1 SWAP program defined in [TRZ⁺23, WCE⁺24]. Since our goal was primarily to analyze the relaxations we presented in our paper we set an upper bound of 600 seconds for the level-1 SWAP program. For examples in which we achieved convergence, the level-1 SWAP program was much slower, often by orders of magnitude. The level-1 SWAP program is an essential ingredient for best known rigorous approximations [LP24] to QMC so the table indicates that our rounding algorithm Algorithm 1 provides practical runtimes for much larger Hamiltonians than previous work.

We also investigated the Shastry-Sutherland model [SS81]. This is a $2d$ model with couplings J along the edges of a $2D$ grid and couplings J_D across the diagonal of each face in the grid (see [WCW⁺19] Eq. 1 for a definition). This model is known to have two phase transitions where the quantum state rapidly changes from one form to another. The first is at $J/J_D \approx 0.65$ and the second at $J/J_D \approx 0.75$. For $J/J_D \leq 0.65$ the ground state is known to be a tensor product of singlets across the diagonal edges of the lattice, while for $J/J_D \geq 0.75$ the state is known to be in the Néel phase corresponding to the product state which maximizes the terms on the square lattice. In between the ground state is a transient plaquette state. Our relaxations mimicked this behavior (see Figure 1) although our relaxations underwent a “phase transition” at different parameter values and the transient regime was much shorter. We can see evidence of this in Figure 3 where we plot the optimal values of different relaxations as well as the ground state energy for a Shastry Sutherland model on 16 qubits. Indeed we can notice a cusp in the objective of our relaxation at $J/J_D = 0.5$ while the exact energy has a cusp at $J/J_D \approx 0.65$. We note that below $J/J_D = 0.5$ all the relaxations considered are correct. The “phase transition” in our relaxations also apparently corresponds to a point at which the relaxations become inexact similar to what was observed in [TRZ⁺23].

Additionally we added disorder to the Shastry-Sutherland model and investigated the objective as a function of disorder. For these models we started at parameter setting where $J/J_D = 0.4$ and multiplied each coupling term by $(1 + \sigma X)$ where σ was a parameter we varied and X was a standard normal random variable. The numerics indicate that the relaxations we have defined are exact for small amounts of disorder and have good performance for even relatively large amounts of disorder. Application of convex optimization hierarchies to studying perturbation theory is a very new and interesting research direction [Has24] and we provide evidence that even the very simple relaxations we have defined are powerful tools for understanding the change in ground state energy under a small perturbation.

We also studied the performance of our relaxations on randomly generated Erdos-Renyi graphs with probability p of edge formation for several values of p in Figure 5 and Table 2. We believe these are important instances to consider for applications of our ideas because heuristics which make use of the structure of the Hamiltonian (i.e. those considered in [WRV⁺23]) will fail on these instances. For dense instances it appears that the SOC program plus level-1 Pauli (denoted $SOC + P1$) has appreciably better performance than just the SOC program Equation (17) and that the level-1 SWAP program has appreciably better performance than the other two. This is seen in both Figure 5 and Table 2 (note that the Hamiltonian in Figure 5 is an affine shift of Table 2). For all the instances we considered we saw reasonable performance with our relaxations indicating that the relaxations are getting within 25% of the optimal value, but we cannot probe very big examples due to the exponential dimension.

model	# edges	SOC	SOC +Pauli-1	Level-1 SWAP	VarBench	Rounded Objective	Comp. Time SOC/SOC+ Pauli-1/Level-1 SWAP (s)
square 16	32	-64	-53.3333	-45.57	-44.9139*	-15.67	0.05/1.5/1.25
square 36	72	-144	-123.4306	-99.76	-97.7576*	-36.01	1.4/2.5/256
square 64	128	-256	-220.1495			-64.86	19/54
square 50	100	-200	-172.405		-135.0204*	-51.04	6.7/27
square 100	200	-400	-344.950		-268.560	-101.87	258/1145
square 196	392	-784	-676.932		-523.983	-199	21357/20024
kagome 18	36	-36	-36	-36	-32.1931*	-10.34	0.08/0.08/1.52
kagome 48	96	-96	-96		-84.2311*	-27.36	2.2/2.7
kagome 75	150	-150	-150			-43.22	11/16
kagome 192	384	-384	-384		-330.143	-110.43	1166/2274
shuriken 24	48	-48	-48	-48	-43.0396*	-13.72	0.18/0.28/7.39
shuriken 96	192	-192	-192		-168.2918	-55	36/44
Pyrochlore 32	96	-120	-109.838	-82.62	-66.15*	-31.77	2.1/3.2/41
Pyrochlore 108	324	-405	-393.133		-210.43	-114.12	592/646
Pyrochlore 256	768	-960	-933.512		-494.69	-271.22	25835/31584

TABLE 1. **Bounds on QMC** for periodic lattices using the scaled Hamiltonian $H = \sum_{(ij) \in E} (XX + YY + ZZ)_{ij}$. Lower bounds include the second order cone (SOC), second order cone plus Pauli Level 1 (SOC+Pauli-1) as well as the Level 1 SWAP hierarchy Rounded objective corresponds to the upper bound obtained through Algorithm 1. In the VarBench column the symbol * indicates that the exact solution was found while the other entries generally correspond to heuristic upper bounds on the ground state energy. We note that square lattice of size 50 is defined differently than the other square lattices, see [WL18] Fig. 5 for a definition. Blank entries under Level-1 SWAP column correspond to lattices which exhausted the computers memory or took longer than the set threshold of 600 seconds to converge.

n	0.2	0.4	0.6	0.8	1
10	1.03	1.12	1.31	1.70	3.00
12	1.04	1.16	1.38	1.92	3.67
14	1.05	1.19	1.44	2.13	4.33
16	1.06	1.21	1.52	2.31	5.00
18	1.07	1.23	1.58	2.47	5.67
20	1.08	1.24	1.64	2.64	6.33
25	1.09	1.28	1.80	2.97	8.00
30	1.11	1.32	1.92	3.27	9.66
35	1.13	1.36	2.02	3.5	11.33
40	1.15	1.42	2.14	3.72	13.00

TABLE 2. Average ratio of the value of the SOC / SOC+Pauli-1 relaxations for random Erdős–Rényi graphs with n where an edge has probability p . We used 500 samples for $n \leq 20$; 100 samples for $n \leq 40$. In VarBench normalization.

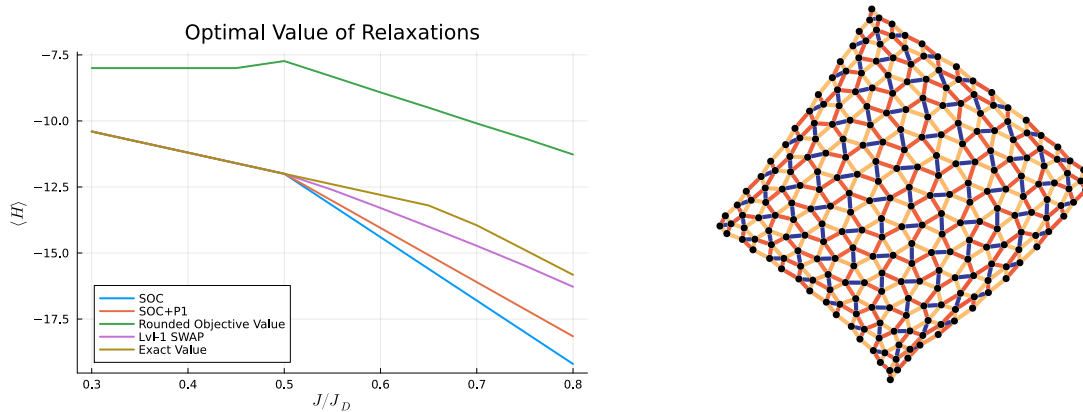


FIGURE 3. Optimal solutions of our relaxations for Shastry-Sutherland models with scaling as in Equation (1). SOC corresponds to Equation (17) and SOC+P1 corresponds to Equation (24). On the Left we plot the optimal solutions versus the exact ground state for a lattice of size 16 qubits where $\langle H \rangle$ indicates the optimal objective whether it be the relaxation or exact solution. On the right a heat map arising from the solution to a 256 qubit disordered instance with parameters $J/J_D = 0.4$ and $\sigma = 0.05$.

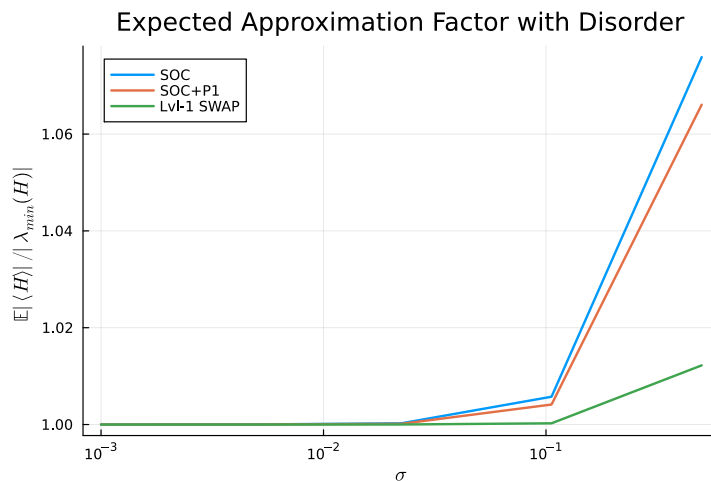


FIGURE 4. Expected approximation factor for Shastry-Sutherland model with disorder with scaling as in Equation (1). $\langle H \rangle$ indicates the optimal value for the SOCP (Equation (17)) or the SOCP supplemented with the first level of the Pauli Hierarchy (Equation (24)). $\lambda_{\min}(H)$ is the ground state energy. All nonzero couplings in the model are multiplied by a factor of $(1 + \sigma X)$ where X is a normally distributed random variable. Average ratio is computed with 1000 samples. The lattice of size size 16.

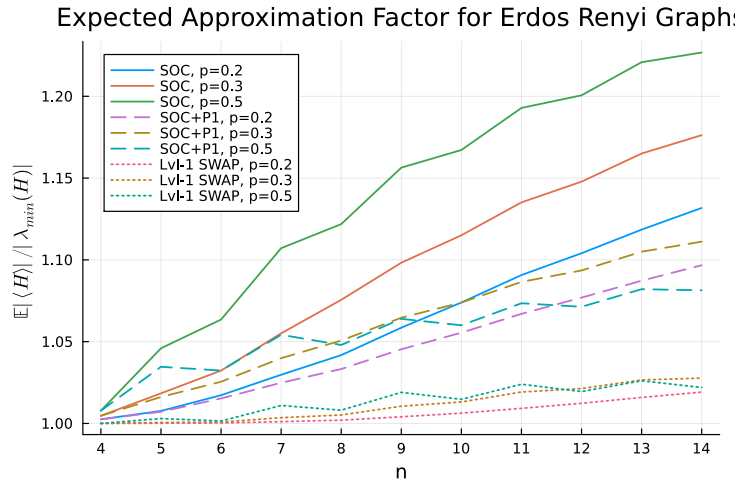


FIGURE 5. Expected approximation factor for Erdos-Renyi graphs of varying sizes with scaling as in Equation (1). $\langle H \rangle$ indicates the optimal value for the SOCP (Equation (17)) or the SOCP supplemented with the first level of the Pauli Hierarchy (Equation (24)). $\lambda_{min}(H)$ is the ground state energy. The probability of edge formation is p and the number of qubits in the graph is n .

APPENDIX A. FOUR QUBITS

We discuss the state conditions for four-qubit marginals.

The analog of the relaxation in Eq. (16) to the quantum max cut problem (1) using mutually consistent four-qubit marginals reads:

$$\begin{aligned}
& \min_{\{\varrho_{ijkl}\}} && -\frac{1}{2} \sum_{(i,j) \in E} \text{tr}((\mathbb{1} - \text{SWAP}_{ij})\varrho_{ij}) \\
& \text{subject to} && \varrho_{ij} = \text{tr}_{k\ell}(\varrho_{ijkl}), \\
& && \varrho_{ijkl} \geq 0 \\
& && \text{tr}(\varrho_{ijkl}) = 1, \\
(48) \quad & && \text{tr}_\ell(\varrho_{ijkl}) = \text{tr}_m(\varrho_{ijkm}), \quad \ell \neq m.
\end{aligned}$$

Above, the sum and constraints are over all pairwise different $i, j, k, \ell, m \in \{1, \dots, n\}$. Denote by

$$(49) \quad x_{ij} = \text{tr}(\varrho_{ij}), \quad x_{ij,kl} = \text{tr}(\varrho_{ij}(kl)).$$

Due to the identity in Eq. (13), all three-body correlations can be expressed in terms of two-body correlations,

$$(50) \quad \langle\langle ijk \rangle\rangle + \langle\langle ikj \rangle\rangle = \langle\langle ij \rangle\rangle + \langle\langle ik \rangle\rangle + \langle\langle jk \rangle\rangle - 1.$$

This implies that the constraint $\text{tr}_\ell(\varrho_{ijkl}) = \text{tr}_m(\varrho_{ijkm})$ for $\ell \neq m$ is mediated through the X_{ij} only, that is the only variables shared by two different marginals are contained in the x_{ij} .

A.1. Four-qubit identities. We now reduce the number of variables further. An analysis of the Gröbner basis given in Ref. [WCE⁺24, Appendix C] shows, in addition to the identity $(123) + (123)^{-1} = (12) + (23) + (13) - \text{id}$ ³ that the remaining identities for S_4 on the subspace of matrices in $\Sigma_{4,2}^{\text{sym}}$ are given by

$$(51) \quad (1234) + (1234)^{-1} = -\text{id} + (13) + (24) + (12)(34) + (14)(23) - (13)(24)$$

and permutations thereof. See also the analytical derivation in Ref. [Pro24]. Together with the three-qubit identity in Eq. (13), this shows that the set of involutions of the form (i, j) and $(i, j)(k, l)$ span $\Sigma_{4,2}^{\text{sym}}$. In fact, a similar result holds for n -partite systems: Procesi has shown that the space $\Sigma_{n,2}^{\text{sym}}$ is spanned by involutions [Pro24].

A.2. State conditions. We are now in position to derive the analogue of Eq. (15), that is the conditions for an operator to be an real invariant four-qubit state. With Eq. (51), consider the positivity condition in Eq. (46) for an invariant operator $A \in \Sigma_{4,2}^{\text{sym}}$

$$(52) \quad P_\lambda \sum_{\sigma \in S_k} \text{tr}(\sigma^{-1}A)R_\lambda(\sigma) \succeq 0$$

for the irreps $\lambda = (4), (3, 1),$ and $(2, 2)$. Appendix B lists orthogonal representations of S_4 . Then the three central Young projectors expand as [see Eq. (38)]

$$\begin{aligned}
P_{(4)} &= \frac{1}{24} \sum_{\pi \in S_4} \pi, \\
P_{(31)} &= \frac{1}{8} \left(3 \text{id} + (12) + (13) + (14) + (23) + (24) + (34) - (12)(34) - (13)(24) - (14)(23) \right. \\
&\quad \left. - (1234) - (1243) - (1342) - (1324) - (1432) - (1423) \right), \\
P_{(22)} &= \frac{1}{12} \left(2(\text{id} + (13)(24) + (14)(23) + (12)(34)) \right. \\
&\quad \left. - (234) - (243) - (123) - (124) - (132) - (134) - (142) - (143) \right).
\end{aligned}$$

³In fact all identities of S_n acting on $(\mathbb{C}^2)^{\otimes n}$ are generated by $\text{id} - (12) - (23) - (13) + (123) + (123)^{-1} = 0$.

On $(\mathbb{C}^2)^{\otimes 4}$ we can variable reduce through the identities in Eq. (13) and (52),

$$\begin{aligned} P_{(4)} &= \frac{1}{12} \left(-3 \text{id} + 2 [(12) + (13) + (14) + (23) + (24) + (34)] + (12)(34) + (13)(24) + (14)(23) \right), \\ P_{(3,1)} &= \frac{1}{4} \left(3 \text{id} - (12)(34) - (13)(24) - (14)(23) \right), \\ P_{(2,2)} &= \frac{1}{6} \left(3 \text{id} - (12) - (13) - (14) - (23) - (24) - (34) + (12)(34) + (13)(24) + (14)(23) \right). \end{aligned}$$

Denote their expectation values by

$$(53) \quad r_{(4)} = \text{tr}(P_{(4)}\varrho), \quad r_{(3,1)} = \text{tr}(P_{(3,1)}\varrho), \quad r_{(2,2)} = \text{tr}(P_{(2,2)}\varrho).$$

Then the normalization condition $\text{tr}(\varrho) = 1$ requires that

$$(54) \quad r_{(4)}, r_{(3,1)}, r_{(2,2)} \geq 0, \quad r_{(4)} + r_{(3,1)} + r_{(2,2)} = 1.$$

The positive semidefinite constraint can be obtained through Proposition D and using the irreducible orthogonal representations given in Appendix B. The conditions for $A \succeq 0$, $A \in \Sigma_4^+$ are, listed by partitions:

$$(\text{Partition } [4]) \quad -3 + 2 [x_{12} + x_{13} + x_{14} + x_{23} + x_{24} + x_{34}] + x_{12,34} + x_{13,24} + x_{14,23} \geq 0;$$

$$(\text{Partition } [3,1]) \quad \begin{pmatrix} A_{00} & A_{01} & A_{02} \\ A_{01} & A_{11} & A_{12} \\ A_{02} & A_{12} & A_{22} \end{pmatrix} \geq 0,$$

where

$$\begin{aligned} A_{00} &= \frac{2}{3} \left(3 + 2 [x_{12} + x_{13} - x_{14} + x_{23} - x_{24} - x_{34}] - x_{12,34} - x_{13,24} - x_{14,23} \right), \\ A_{01} &= \frac{\sqrt{2}}{3} \left(-2x_{12} + x_{13} - x_{14} + x_{23} - x_{24} + 2x_{34} + 4x_{12,34} - 2x_{13,24} - 2x_{14,23} \right), \\ A_{02} &= \frac{\sqrt{6}}{3} \left(-x_{13} - x_{14} + x_{23} + x_{24} + 2x_{13,24} - 2x_{14,23} \right), \\ A_{11} &= \frac{2}{3} \left(3 + x_{12} - x_{34} + 2x_{24} - 2x_{13} + 2x_{14} - 2x_{23} + x_{12,34} - 2x_{13,24} - 2x_{14,23} \right), \\ A_{12} &= \frac{2}{\sqrt{3}} \left(-x_{13} - x_{14} + x_{23} + x_{24} - x_{13,24} + x_{14,23} \right), \\ A_{22} &= 2 \left(1 - x_{12} - x_{12,34} + x_{34} \right); \end{aligned}$$

and

$$(\text{Partition } [2,2]) \quad \begin{pmatrix} B_{00} & B_{01} \\ B_{01} & B_{11} \end{pmatrix} \geq 0,$$

where

$$(55) \quad \begin{aligned} B_{00} &= 3 + x_{12} - 2x_{13} - 2x_{14} - 2x_{23} - 2x_{24} + x_{34} - x_{12,34} + 2x_{13,24} + 2x_{14,23}, \\ B_{01} &= \sqrt{3} \left(-x_{13} + x_{14} + x_{23} - x_{24} + x_{13,24} - x_{14,23} \right), \\ B_{11} &= 3 \left(1 - x_{12} - x_{34} + x_{12,34} \right). \end{aligned}$$

These correspond to the fact that a state is positive semidefinite on the irreducible representations corresponding to (4), (3, 1), and (2, 2) respectively.

A.3. Second order cone formulation. As in the three-qubit case, the condition of (Partition [2,2]) can be formulated as a second-order cone constraint. The corresponding subnormalized real Bloch ball reads:

$$(56) \quad B = \begin{pmatrix} b_0 + b_1 & b_2 \\ b_2 & b_0 - b_1 \end{pmatrix} \succeq 0.$$

with $b_0 = (B_{00} + B_{11})/2$, $b_1 = (B_{00} - B_{11})/2$, $b_2 = B_{01}$. Then

$$(57) \quad \begin{aligned} b_0 &= \frac{1}{6} \left(3 - x_{12} - x_{13} - x_{14} - x_{23} - x_{24} - x_{34} + x_{12,34} + x_{13,24} + x_{14,23} \right), \\ b_1 &= 2x_{12} - 2x_{12,34} - x_{13} + x_{13,24} - x_{14} + x_{14,23} - x_{23} - x_{24} + 2x_{34} \\ b_2 &= \sqrt{3} \left(-x_{13} + x_{14} + x_{23} - x_{24} + x_{13,24} - x_{14,23} \right). \end{aligned}$$

We use the fact that

$$(58) \quad \begin{pmatrix} b_0 + b_1 & b_2 \\ b_2 & b_0 - b_1 \end{pmatrix} \geq 0 \quad \iff \quad b_1^2 + b_2^2 \leq b_0^2, \quad b_0 + b_1 \geq 0, \quad b_0 - b_1 \geq 0.$$

Remark 7. Also the 3×3 semidefinite constraint from the partition [3, 1] can be relaxed to a second-order cone constraint by imposing that all of its 2×2 minors are positive semidefinite. This does not seem to give a computational speed-up.

APPENDIX B. IRREDUCIBLE REPRESENTATIONS OF S_3 AND S_4

We list the orthogonal irreducible representations R_λ of S_3 and S_4 below. These are needed to obtain the decomposition in terms of x_{ij} and $x_{ij,kl}$ in Appendix A.

S₃. The symmetric group S_3 has three irreps labeled by partitions [3], [2, 1], and [1, 1, 1]. Of these, the first two are non-zero while the sign representation [1, 1, 1] vanishes on $(\mathbb{C}^2)^{\otimes 3}$.

λ	id	(12)	(23)	(13)	(123)	(132)
[3]	1	1	1	1	1	1
[2, 1]	$\begin{pmatrix} 1 & 0 \\ 0 & 1 \end{pmatrix}$	$\begin{pmatrix} 1 & 0 \\ 0 & -1 \end{pmatrix}$	$\frac{1}{2} \begin{pmatrix} -1 & \sqrt{3} \\ \sqrt{3} & 1 \end{pmatrix}$	$\frac{1}{2} \begin{pmatrix} -1 & -\sqrt{3} \\ -\sqrt{3} & 1 \end{pmatrix}$	$\frac{1}{2} \begin{pmatrix} -1 & \sqrt{3} \\ -\sqrt{3} & -1 \end{pmatrix}$	$\frac{1}{2} \begin{pmatrix} -1 & -\sqrt{3} \\ \sqrt{3} & -1 \end{pmatrix}$
[1, 1, 1]	1	-1	-1	-1	1	1

S₄. The symmetric group S_4 has irreducible representation labeled by the partitions [4], [3, 1], [2, 2], [2, 1, 1], [1, 1, 1, 1]. Of these, by the Schur-Weyl duality only [4], [3, 1], and [2, 2] are nonvanishing, these having no more than 2 rows. The completely symmetric irrep [4] is trivial, having value $R_{[4]}(\pi) = 1$ for all $\pi \in S_4$. We list the remaining nonvanishing irreps below. Again we can do variable reduction, and Appendix B in Ref. [WCE⁺24] together with the fact that Quantum Max Cut is real shows that the variables (i, j) and $(i, j)(k, l)$ span the space of permutations on $(\mathbb{C}^d)^{\otimes 4}$.

Partition	Permutation (all after * redundant on $(\mathbb{C}^2)^{\otimes 4}$)	Irreducible Representation
[3, 1]	id;	$\begin{pmatrix} 1 & 0 & 0 \\ 0 & 1 & 0 \\ 0 & 0 & 1 \end{pmatrix}$
	(13)(24);	$-\frac{1}{3} \begin{pmatrix} 1 & \sqrt{2} & -\sqrt{6} \\ \sqrt{2} & 2 & \sqrt{3} \\ -\sqrt{6} & \sqrt{3} & 0 \end{pmatrix}$

$$\begin{array}{ll}
(14)(23); & -\frac{1}{3} \begin{pmatrix} 1 & \sqrt{2} & \sqrt{6} \\ \sqrt{2} & 2 & -\sqrt{3} \\ \sqrt{6} & -\sqrt{3} & 0 \end{pmatrix} \\
(12)(34); & \frac{1}{3} \begin{pmatrix} -1 & 2\sqrt{2} & 0 \\ 2\sqrt{2} & 1 & 0 \\ 0 & 0 & -3 \end{pmatrix} \\
* (234); (243); & \frac{1}{6} \begin{pmatrix} -2 & \sqrt{2} & \sqrt{6} \\ \sqrt{2} & -1 & 2\sqrt{3} \\ \sqrt{6} & 2\sqrt{3} & 3 \end{pmatrix} \\
* (132); (123); & \frac{1}{2} \begin{pmatrix} 2 & 0 & 0 \\ 0 & -1 & 0 \\ 0 & 0 & -1 \end{pmatrix} \\
* (143); (134); & -\frac{1}{6} \begin{pmatrix} 2 & -\sqrt{2} & \sqrt{6} \\ -\sqrt{2} & 1 & 2\sqrt{3} \\ \sqrt{6} & 2\sqrt{3} & -3 \end{pmatrix} \\
* (124); (142); & \frac{1}{6} \begin{pmatrix} -2 & -2\sqrt{2} & 0 \\ -2\sqrt{2} & 5 & 0 \\ 0 & 0 & -3 \end{pmatrix} \\
(34); & \frac{1}{3} \begin{pmatrix} -1 & 2\sqrt{2} & 0 \\ 2\sqrt{2} & 1 & 0 \\ 0 & 0 & 3 \end{pmatrix} \\
* (1324); (1423); & -\frac{1}{3} \begin{pmatrix} 1 & \sqrt{2} & 0 \\ \sqrt{2} & 2 & 0 \\ 0 & 0 & 0 \end{pmatrix} \\
(12); & \begin{pmatrix} 1 & 0 & 0 \\ 0 & 1 & 0 \\ 0 & 0 & -1 \end{pmatrix} \\
(23); & \frac{1}{2} \begin{pmatrix} 2 & 0 & 0 \\ 0 & -1 & \sqrt{3} \\ 0 & \sqrt{3} & 1 \end{pmatrix} \\
* (1342); (1243); & \frac{1}{6} \begin{pmatrix} -2 & \sqrt{2} & \sqrt{6} \\ \sqrt{2} & -1 & -\sqrt{3} \\ \sqrt{6} & -\sqrt{3} & -3 \end{pmatrix} \\
(14); & -\frac{1}{6} \begin{pmatrix} 2 & 2\sqrt{2} & 2\sqrt{6} \\ 2\sqrt{2} & -5 & \sqrt{3} \\ 2\sqrt{6} & \sqrt{3} & -3 \end{pmatrix}
\end{array}$$

(24);		$\frac{1}{6} \begin{pmatrix} -2 & -2\sqrt{2} & 2\sqrt{6} \\ -2\sqrt{2} & 5 & \sqrt{3} \\ 2\sqrt{6} & \sqrt{3} & 3 \end{pmatrix}$
(13);		$\frac{1}{2} \begin{pmatrix} 2 & 0 & 0 \\ 0 & -1 & -\sqrt{3} \\ 0 & -\sqrt{3} & 1 \end{pmatrix}$
* (1432); (1234);		$-\frac{1}{6} \begin{pmatrix} 2 & -\sqrt{2} & \sqrt{6} \\ -\sqrt{2} & 1 & -\sqrt{3} \\ \sqrt{6} & -\sqrt{3} & 3 \end{pmatrix}$
<hr/>		
[2, 2]	id; (13)(24); (14)(23); (12)(34);	$\begin{pmatrix} 1 & 0 \\ 0 & 1 \end{pmatrix}$
	* (234); (132); (143); (124); (243); (134); (142); (123);	$-\frac{1}{2} \begin{pmatrix} 1 & 0 \\ 0 & 1 \end{pmatrix}$
	(34); (12); * (1324); (1423);	$\begin{pmatrix} 1 & 0 \\ 0 & -1 \end{pmatrix}$
	(23); (1342); (14); (1243);	$\frac{1}{2} \begin{pmatrix} -1 & \sqrt{3} \\ \sqrt{3} & 1 \end{pmatrix}$
	(24); (13); * (1432); (1234);	$\frac{1}{2} \begin{pmatrix} -1 & -\sqrt{3} \\ -\sqrt{3} & 1 \end{pmatrix}$
<hr/>		

REFERENCES

- [AG03] F. Alizadeh and D. Goldfarb. Second-order cone programming. *Mathematical Programming*, 95:3–51, 2003.
- [AGM20] Anurag Anshu, David Gosset, and Karen Morenz. Beyond product state approximations for a quantum analogue of max cut. Schloss Dagstuhl - Leibniz-Zentrum für Informatik, 2020.
- [AS48] Milton Abramowitz and Irene A Stegun. *Handbook of mathematical functions with formulas, graphs, and mathematical tables*, volume 55. US Government printing office, 1948.
- [BGSV12] Christine Bachoc, Dion C. Gijswijt, Alexander Schrijver, and Frank Vallentin. *Handbook on Semidefinite, Conic and Polynomial Optimization*, volume 166 of *International Series in Operations Research & Management Science*, chapter Invariant Semidefinite Programs. Springer, Boston, MA, 2012.
- [BH12] Thomas Barthel and Robert Hübener. Solving condensed-matter ground-state problems by semidefinite relaxations. *Physical Review Letters*, 108(20), may 2012.
- [BH16] Fernando GSL Brandao and Aram W Harrow. Product-state approximations to quantum states. *Communications in Mathematical Physics*, 342:47–80, 2016.
- [BOFV14] Jop Briët, Fernando Mário de Oliveira Filho, and Frank Vallentin. Grothendieck inequalities for semidefinite programs with rank constraint. *Theory of Computing*, 10(4):77–105, 2014.
- [BP12] Tillmann Baumgratz and Martin B Plenio. Lower bounds for ground states of condensed matter systems. *New Journal of Physics*, 14(2):023027, feb 2012.
- [CA86] David Ceperley and Berni Alder. Quantum monte carlo. *Science*, 231(4738):555–560, 1986.
- [CJK⁺23] Charlie Carlson, Zackary Jorquera, Alexandra Kolla, Steven Kordonowy, and Stuart Wayland. Approximation algorithms for quantum max- d -cut. *arXiv:2309.10957*, 2023.
- [CS06] Benoît Collins and Piotr Śniady. Integration with respect to the Haar measure on unitary, orthogonal and symplectic group. *Communications in Mathematical Physics*, 264:773–795, 2006.
- [CT17] Giuseppe Carleo and Matthias Troyer. Solving the quantum many-body problem with artificial neural networks. *Science*, 355(6325):602–606, 2017.
- [EW01] Tilo Eggeling and Reinhard F. Werner. Separability properties of tripartite states with $U \otimes U \otimes U$ symmetry. *Physical Review A*, 63:042111, Mar 2001.
- [Faw19] Hamza Fawzi. On representing the positive semidefinite cone using the second-order cone. *Mathematical Programming*, 175:109–118, 2019.

- [Fuk07] Large-scale semidefinite programs in electronic structure calculation. *Mathematical Programming*, 109:553–580, 2007.
- [GP19] Sevag Gharibian and Ojas Parekh. Almost Optimal Classical Approximation Algorithms for a Quantum Generalization of Max-Cut. In Dimitris Achlioptas and László A. Végh, editors, *Approximation, Randomization, and Combinatorial Optimization. Algorithms and Techniques (APPROX/RANDOM 2019)*, volume 145 of *Leibniz International Proceedings in Informatics (LIPIcs)*, pages 31:1–31:17, Dagstuhl, Germany, 2019. Schloss Dagstuhl–Leibniz-Zentrum fuer Informatik.
- [Has24] Matthew B. Hastings. Perturbation theory and the sum of squares. *2205.12325*, 2024.
- [HNP⁺23] Yeongwoo Hwang, Joe Neeman, Ojas Parekh, Kevin Thompson, and John Wright. Unique games hardness of quantum max-cut, and a conjectured vector-valued Borell’s inequality. In *Proceedings of the 2023 Annual ACM-SIAM Symposium on Discrete Algorithms (SODA)*, pages 1319–1384. SIAM, 2023.
- [Kin23] Robbie King. An Improved Approximation Algorithm for Quantum Max-Cut on Triangle-Free Graphs. *Quantum*, 7:1180, November 2023.
- [KSDN22] Ilya Kull, Norbert Schuch, Ben Dive, and Miguel Navascués. Lower bounding ground-state energies of local hamiltonians through the renormalization group. *2212.03014*, 2022.
- [Lee22] Eunou Lee. Optimizing quantum circuit parameters via sdp. In *33rd International Symposium on Algorithms and Computation (ISAAC 2022)*. Schloss-Dagstuhl-Leibniz Zentrum für Informatik, 2022.
- [LP24] Eunou Lee and Ojas Parekh. An improved quantum max cut approximation via maximum matching. In *51st International Colloquium on Automata, Languages, and Programming (ICALP 2024)*. Schloss Dagstuhl–Leibniz-Zentrum für Informatik, 2024.
- [LSM19] Andreas M. Läuchli, Julien Sudan, and Roderich Moessner. $s = \frac{1}{2}$ kagome Heisenberg antiferromagnet revisited. *Physical Review B*, 100:155142, Oct 2019.
- [LVBL98] Miguel Sousa Lobo, Lieven Vandenbergh, Stephen Boyd, and Hervé Lebret. Applications of second-order cone programming. *Linear Algebra and its Applications*, 284(1):193–228, 1998. International Linear Algebra Society (ILAS) Symposium on Fast Algorithms for Control, Signals and Image Processing.
- [Maz09] David A. Mazziotti. *Reduced-Density-Matrix Mechanics: With Application to Many-Electron Atoms and Molecules*. Advances in Chemical Physics. John Wiley & Sons, Inc., 2009.
- [NNE⁺01] Maho Nakata, Hiroshi Nakatsuji, Masahiro Ehara, Mitsuhiro Fukuda, Kazuhide Nakata, and Katsuki Fujisawa. Variational calculations of fermion second-order reduced density matrices by semidefinite programming algorithm. *The Journal of Chemical Physics*, 114(19):8282–8292, 05 2001.
- [NPA08] Miguel Navascués, Stefano Pironio, and Antonio Acín. A convergent hierarchy of semidefinite programs characterizing the set of quantum correlations. *New J. Phys.*, 10(7):073013, 2008.
- [Orú19] Román Orús. Tensor networks for complex quantum systems. *Nature Reviews Physics*, 1(9):538–550, aug 2019.
- [PNA10] S. Pironio, M. Navascués, and A. Acín. Convergent relaxations of polynomial optimization problems with noncommuting variables. *SIAM J. Opt.*, 20(5):2157–2180, 2010.
- [Pro07] Claudio Procesi. *Lie Groups, An Approach through Invariants and Representations*. Springer-Verlag New York, 2007.
- [Pro21] Claudio Procesi. A note on the Formanek Weingarten function. *Note di Matematica*, 41, 2021.
- [Pro24] Claudio Procesi. Some special bases of the 2-swap algebras. *arXiv:2406.18687*, 2024.
- [PT21] Ojas Parekh and Kevin Thompson. Application of the level-2 quantum Lasserre hierarchy in quantum approximation algorithms. Schloss Dagstuhl - Leibniz-Zentrum für Informatik, 2021.
- [PT22] Ojas Parekh and Kevin Thompson. An optimal product-state approximation for 2-local quantum hamiltonians with positive terms. *arXiv:2206.08342*, 2022.
- [SA90] Hanif D Sherali and Warren P Adams. A hierarchy of relaxations between the continuous and convex hull representations for zero-one programming problems. *SIAM Journal on Discrete Mathematics*, 3(3):411–430, 1990.
- [SS81] B. Sriram Shastry and Bill Sutherland. Exact ground state of a quantum mechanical antiferromagnet. *Physica B+C*, 108(1):1069–1070, 1981.
- [TRZ⁺23] Jun Takahashi, Chaithanya Rayudu, Cunlu Zhou, Robbie King, Kevin Thompson, and Ojas Parekh. An su(2)-symmetric semidefinite programming hierarchy for quantum max cut. *arXiv:2307.15688*, 2023.
- [WCE⁺24] Adam Bene Watts, Anirban Chowdhury, Aidan Epperly, J. William Helton, and Igor Klep. Relaxations and Exact Solutions to Quantum Max Cut via the Algebraic Structure of Swap Operators. *Quantum*, 8:1352, May 2024.
- [WCW⁺19] Alexander Wietek, Philippe Corboz, Stefan Wessel, Bruce Normand, Frédéric Mila, and Andreas Honecker. Thermodynamic properties of the Shastry-Sutherland model throughout the dimer-product phase. *Physical Review Research*, 1(3):033038, 2019.
- [WL18] Alexander Wietek and Andreas M. Läuchli. Sublattice coding algorithm and distributed memory parallelization for large-scale exact diagonalizations of quantum many-body systems. *Physical Review E*, 98:033309, Sep 2018.

- [WRV⁺23] Dian Wu, Riccardo Rossi, Filippo Vicentini, Nikita Astrakhantsev, Federico Becca, Xiaodong Cao, Juan Carrasquilla, Francesco Ferrari, Antoine Georges, Mohamed Hibat-Allah, Masatoshi Imada, Andreas M. Läuchli, Guglielmo Mazzola, Antonio Mezzacapo, Andrew Millis, Javier Robledo Moreno, Titus Neupert, Yusuke Nomura, James Nys, Olivier Parcollet, Rico Pohle, Imelda Romero, Michael Schmid, J. Maxwell Silvester, Sandro Sorella, Luca F. Tocchio, Lei Wang, Steven R. White, Alexander Wietek, Qi Yang, Yiqi Yang, Shiwei Zhang, and Giuseppe Carleo. Variational benchmarks for quantum many-body problems. *arXiv:2302.04919*, 2023.

INSTITUTE OF THEORETICAL PHYSICS AND ASTROPHYSICS, UNIVERSITY OF GDAŃSK, POLAND
Email address: `felix.huber@ug.edu.pl`

SANDIA NATIONAL LABORATORIES, ALBUQUERQUE, U.S.A.
Email address: `kevthom@sandia.gov`

SANDIA NATIONAL LABORATORIES, ALBUQUERQUE, U.S.A.
Email address: `odparek@sandia.gov`

DEPARTMENT OF COMPUTER SCIENCE, AND INSTITUTE FOR PHOTONIC QUANTUM SYSTEMS, PADERBORN UNIVERSITY, GERMANY.
Email address: `sevag.gharibian@upb.de`